uc3m | Universidad Carlos III de Madrid

University Degree in Energy Engineering
Academic Year (2020-2021)

Bachelor Thesis

"Photoelectric characterization of solar cells based on III-V semiconductors"

Natalia Gómez Gámez

Supervisor

Elisa García-Tabarés Valdivieso

Madrid, September 2021

ABSTRACT

This bachelor thesis is focused on the theoretical background study and its subsequent experimental application of solar cells based on III-V semiconductors with the aim of understanding the relationship between the band-gap of the materials and their electrical performance (i.e. quantum efficiency). Furthermore, the effect of the material's properties on the quantum efficiency is analysed, with the aim of optimizing the parameters to improve the efficiency of future solar devices. These III-V semiconductors that have excellent properties and different ranges of band-gap are connected in series forming multi-junction solar cells. Thus, the light that is not absorbed by the upper layers is absorbed in the lower layers, so with this type of cells the fitting of the solar devices to the solar spectrum is improved.

Through the characterization of the tested III-V solar cells using a spectral response measurement equipment, it was proved that as the band-gap energy decreases, the quantum efficiency increases as does the absorption of light wavelengths available, so the greater the energy of the band-gap, the smaller the efficiencies reached.

A different approach for a potential increase of the solar cell efficiency is also described and used during this project. This approach is based on a simulation tool. Thanks to those simulations, the effect of different modular parameters on the performance of the devices has been studied and the obtained results can be applied in the manufacture of future devices. Moreover, this study can be used as a feedback tool for upcoming experimental research.

Keywords: III-V solar cells, characterization, spectral response, quantum efficiency, solar spectrum, band-gap.

ACKNOWLEDGEMENTS

I want to start by thanking Elisa García-Tabarés Valdivieso, who has been helping me with great dedication in every step during the development of this project. It has been a pleasure working with you throughout this time. Thank you for always being available and giving me the opportunity to have a first contact with the research world.

I want to thank all those people who have been by my side during these last years, to those who are close day-to-day and those who are a little further away but seem to be here, to the friends who have always been there and the ones who I have met in college. Thank you for making this journey unforgettable and always helping me through tough times.

Last but of course not least, thank my family for their unconditional support, for having given me everything I need to get here, because without their help it would not have been possible to achieve everything I have reached today.

For these reasons, thank you all.

CONTENTS

LIST OF FIGURES

LIST OF TABLES

CHAPTER 1
INTRODUCTION

1. INTRODUCTION

1.1 Background

1.1.1 Current problematic of the energy model

The world energy situation is at a very difficult point, i.e. the demand of energy is continuously increasing, and the current energy model is based on the use of fossil fuels (oil, gas and their derivatives such as gasoline and diesel), whose resources are limited. Moreover, the emissions emitted when burning these fuels are mainly greenhouse gases that are changing the composition of the Earth's atmosphere and are one of the mean causes of climate change.

These emissions began after the so-called Industrial Revolution because of the use of fossil fuels in the industry. From then until now the atmospheric concentrations of carbon dioxide (CO_2) have been increasing except for some episodes produced by great world disasters as it is represented in figure 1.1, where the global energy-related[1] CO_2 emissions along the years are represented [1].

The biggest shock to the global energy system was last year 2020 due to the COVID-19 pandemic that also resulted in a decrease of the carbon emissions of almost 8% during the months of January to April as we can see on the left side of the graph below [2-3].

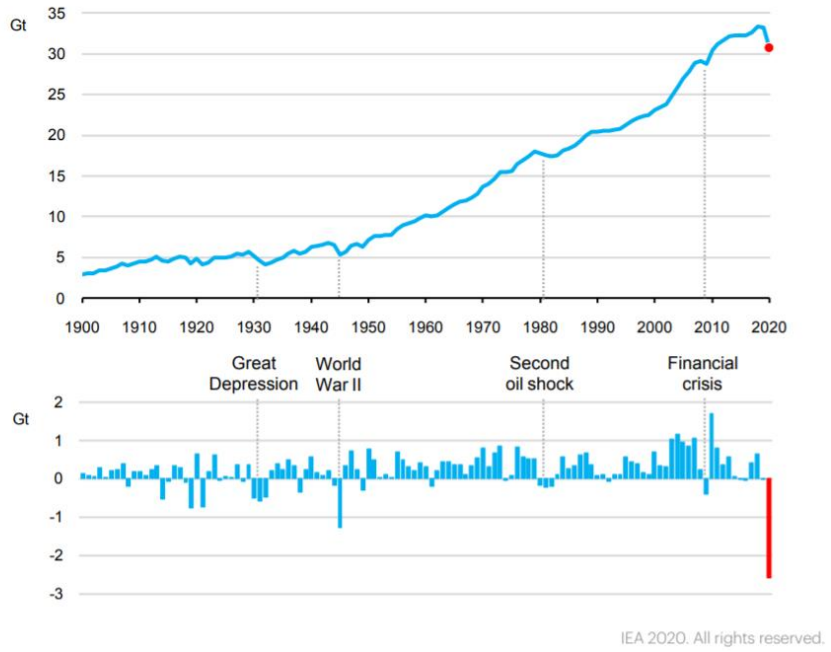

Figure 1.1 GLOBAL ENERGY-RELATED CO_2 EMISSIONS, 1900-2020 [3].

[1] In the International Energy Outlook 2016 book, energy-related CO_2 emissions are defined as emissions related to the combustion of fossil fuels (liquid fuels, natural gas, and coal) and emissions associated with petroleum feedstocks. Emissions from the flaring of natural gas are not included [4].

Energy accounts for two-thirds of total greenhouse gasses and the problems that these generate are promoting the emergence of policy measurements aimed to reduce emissions and encourage sustainable development to mitigate climate change [3].

The Paris Agreement, whose objective is to limit global warming below 2 ºC compared with pre-industrial levels, has activated a global action for climate. Governments and society in general are demanding changes in the production of energy trying to achieve more efficient and environmentally friendly manners [5-6]. For instance, the European Union aims to have an economy with zero greenhouse gas emissions in 2050. To reach this final result, partial objectives have been set in 2020 and 2030 to attain the planned goal [7].

The targets of the 20-20-20 strategy stated that by 2020, there must be a 20% reduction in greenhouse gas emissions from 1990 levels, 20% of the energy consumed in Europe has to come from renewable energies and the energy efficiency has to be improved by 20% [8]. The 2030 objectives are more demanding since they are closest to 2050 and the European commission proposed last year to set the greenhouse gas emissions up to at least 55% with respect to 1990, a 32% of the energy must come from renewable energies and the energy efficiency has to reach a 32.5% [9].

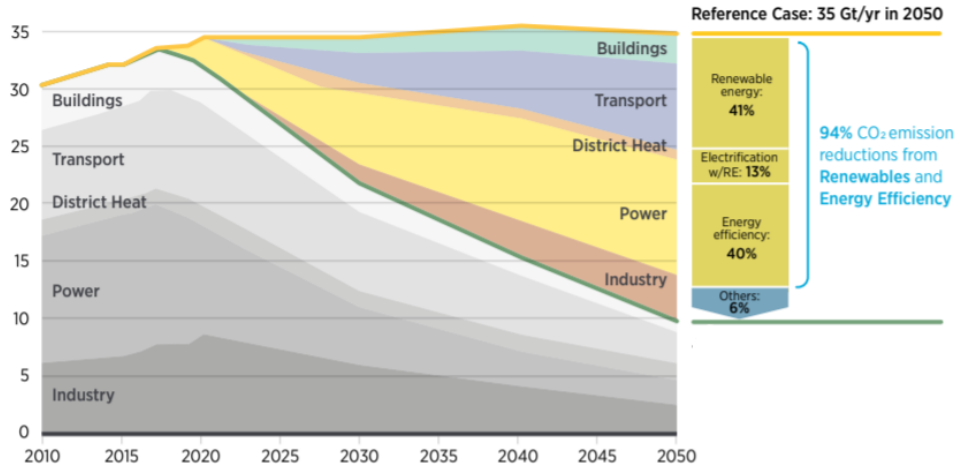

Figure 1.2 ANNUAL ENERGY-RELATED CO_2 EMISSIONS AND REDUCTIONS, 2015-2050 (Gt/year) [10].

The combination of the targets of renewable energy and energy efficiency can provide over 90% of the carbon emission reductions as it is shown in the reference case shown in figure 1.2. Therefore, renewable energies play a very important role in this transition to the net-zero emissions plan. Consequently, all possible renewable sources are worthwhile, represented with its growth in figure 1.3 with an estimation for 2050. There we can see that solar energy will be one of the best options to cover part of the global energy demand as it works with solar radiation, and it can be transformed into energy in several ways [10].

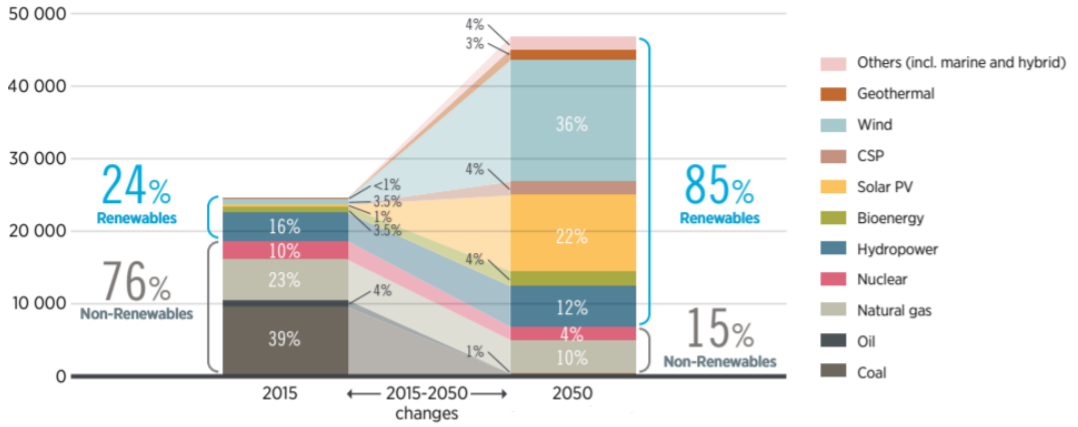

Figure 1.3 BREAKDOWN OF ELECTRICITY GENERATION BY SOURCE (TWh/year) [10].

1.1.2 State of the art of solar energy

Photovoltaic energy started to be researched more thoroughly in the 1970s, coinciding with the first international energy crisis. From that moment starts the huge development of that energy source that uses sunlight as raw material, its characteristics, and potential applications. Nowadays, PV energy is currently a field with a wide range of scientific and technological development. One of the main focuses of the studies related to solar energy is to increase the efficiency of the solar cells by trying new materials and the combination of them to obtain better results [11].

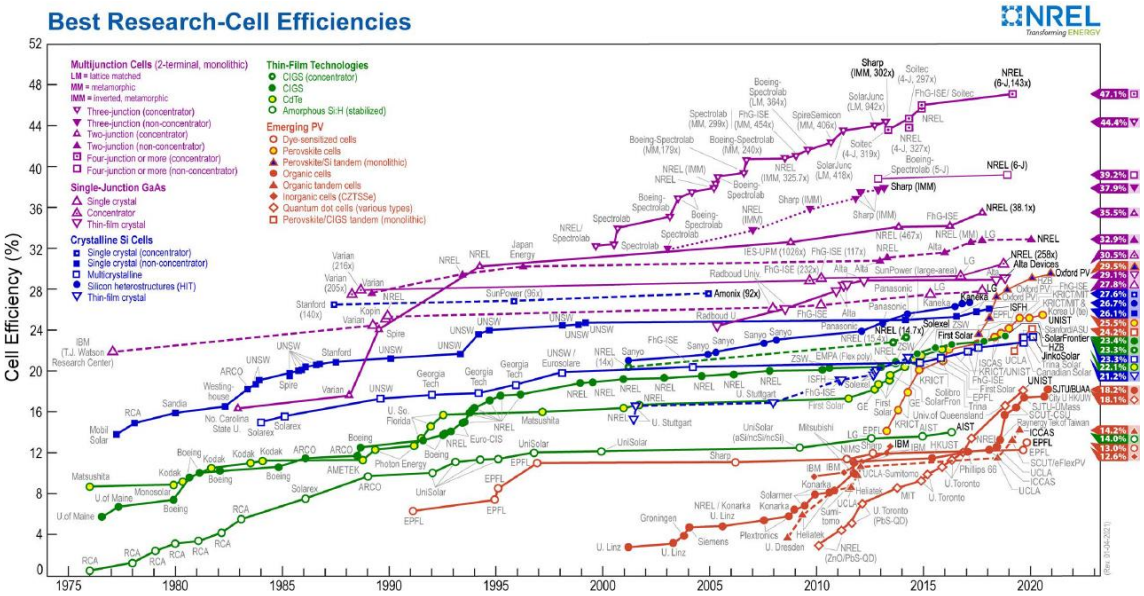

Figure 1.4 SOLAR CELL EFFICIENCY EVOLUTION FOR DIFFERENT TECHNOLOGIES [12].

By observing figure 1.4 it can be seen the evolution of the efficiency of the solar cells along the years, starting in 1976 with values between 1% and 9% with thin-film

technologies until nowadays, obtaining the maximum efficiency of 47.1% [12] with multi-junction cells. Going through a big increase around 1990.

Despite the COVID-19 pandemic the PV market grew significantly in 2020. At least 139.4 GW were installed and commissioned in the world. Having a total installed capacity for PV of about 760 GW at the end of the year [13]. For this year 2021, a new record for capacity additions is expected, with nearly 117 GW installed, a nearly 10% rise from 2020. Going further, it is expected that the expansion after 2022 is going to be more accelerated because of the policy support and the cost reductions. All these additions are depicted in figure 1.5, separated by colours in each region. Analysing the parts of the bars we can see that the greatest expansion is occurring in China, followed by Europe and the United States [14].

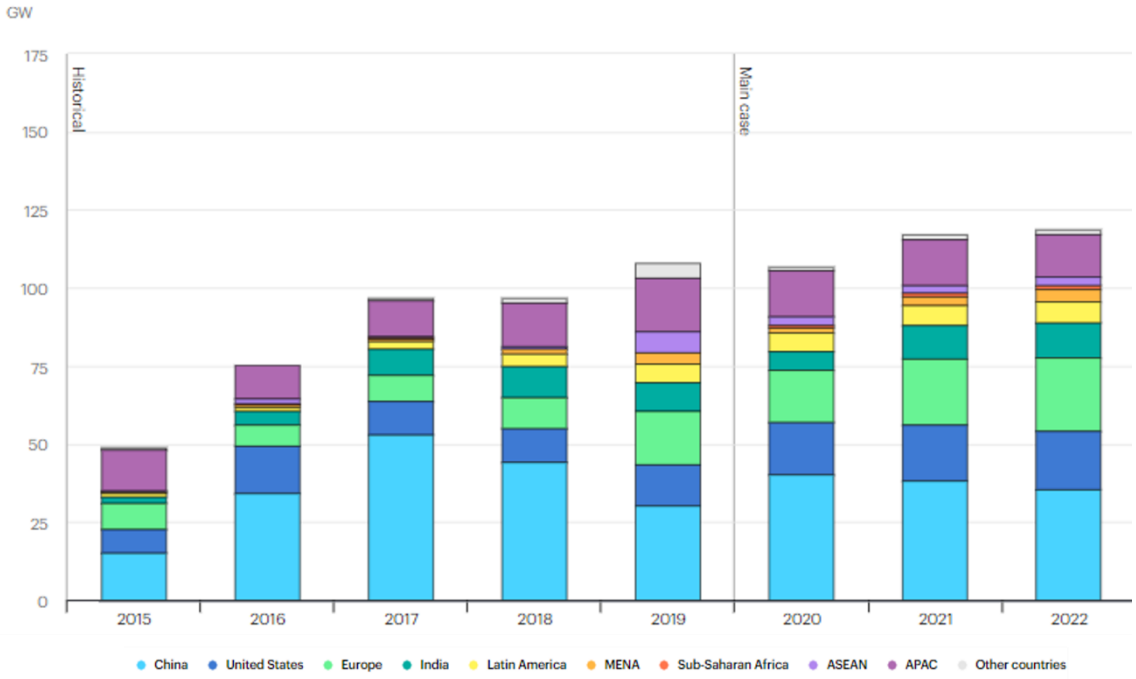

Figure 1.5 SOLAR PV NET CAPACITY ADDITIONS BY REGION, 2015-2022 [14].

As it was shown in figure 1.4 and it is going to be explained in more detail in the following chapter, photovoltaic cells (PV), can be made with different characteristics and are divided into different technologies that can be classified into three generations according to their technical attributes.

The first generation of PV cells is composed of monocrystalline and polycrystalline silicon cells, all of them manufactured with a single-junction structure. Monocrystalline cells are made from a single pure crystal of silicon with almost no defects or impurities. They have high efficiencies and high prices due to the purity of the material. On the other hand, polycrystalline silicon cells are manufactured with ingots of multi-crystalline silicon. Obtaining less efficiencies than monocrystalline cells and with a cheaper price as they are easier to manufacture.

Nowadays, the prices of silicon cells have been greatly reduced, but still have limited efficiencies as we can see in graph 1.6.

Second generation of PV cells are still made by a single-junction structure, but the efficiencies and manufacturing costs compared with the first generation are reduced. This generation is usually manufactured by thin-film technologies that are made from very thin layers of semiconductor materials. In this generation we can differentiate between three types: amorphous silicon, Cadmium Telluride (CdTe) and Copper Indium Gallium Selenide (CIGS).

First-generation cells are the most widely used among the photovoltaic industry, followed by the second-generation cells but they are the ones with high efficiencies but higher prices.

Third generation solar cells are the so-called emerging generations, its aim is to achieve the lowest possible price and far greater efficiencies than previous generations. This generation is going to be explained in more detail in section 1.1.3 [15].

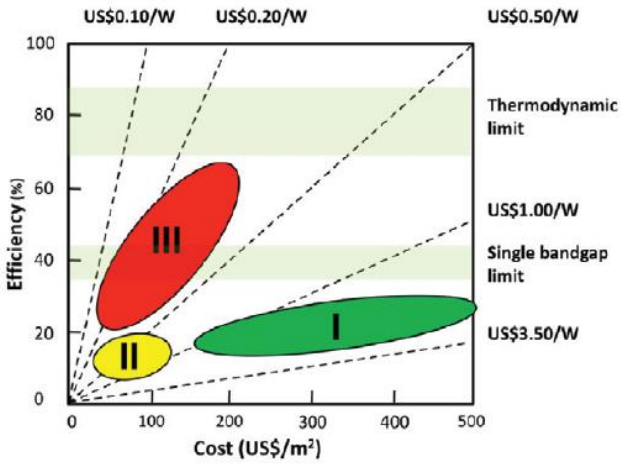

Figure 1.6 COST AND POTENTIAL EFFICIENCY OF ALL THREE GENERATION PHOTOVOLTAIC TECHNOLOGIES [16].

Cost per Watt of the various technologies varies significantly, as seen in figure 1.6. First-generation cells are reasonably efficient but the most expensive; second-generation cells are cheaper but have lower efficiencies; and third-generation cells are still in development but have the potential to attain higher efficiencies at reduced costs.

We can also observe in this graph that only the third generation achieves the theoretical efficiency of a perfect single-junction solar cell, which is referred to as the single band-gap limit [17].

1.1.3 Emerging generations

Third-generation cells are a generation that is now under research and they are considered as the emerging photovoltaics. They used thin-film technologies as in the second generation of photovoltaics but with the aim of achieving more efficient devices at a cheap production cost by using a variety of new materials [18].

Inside this generation there are different types of solar cells that are highlighted in figure 1.7 and also represented in pink colour in figure 1.4 as multi-junction cells, that since being a large group, NREL has separated them from the emerging PV cells although they also belong to this group [19].

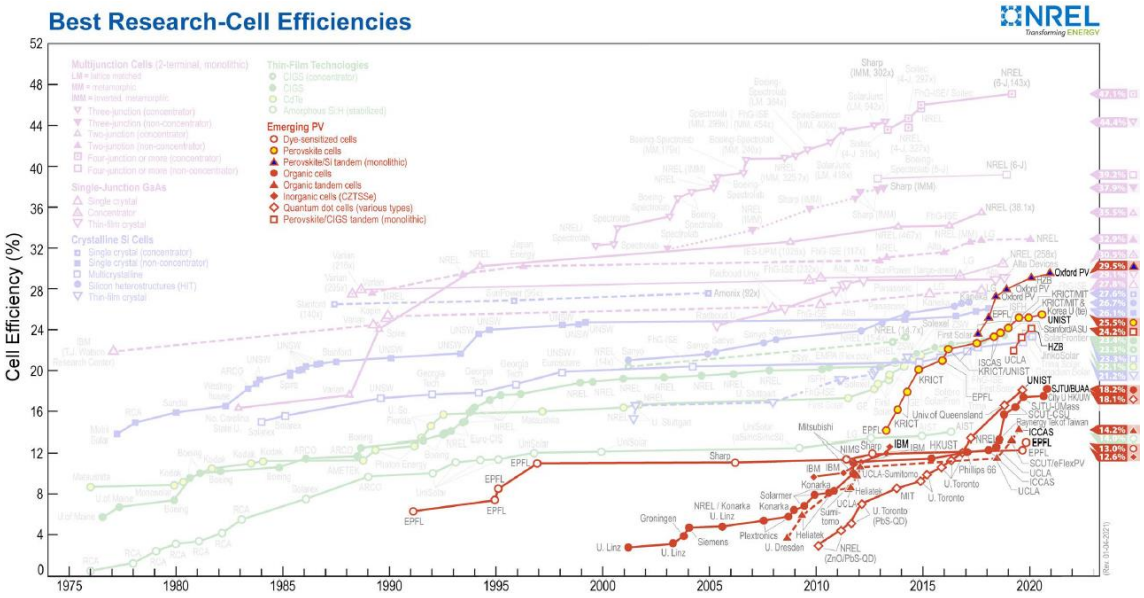

Figure 1.7 SOLAR CELL EFFICIENCY EVOLUTION FOR EMERGING TECHNOLOGIES [19].

Dye-sensitized solar cells (DSSCs) are a type of cells that have been investigated for more than two decades increasing their efficiency from around 4% until nowadays that the record is in an efficiency of 13%. They use oxide semiconductors that are materials with low toxicity and can work with wide band-gaps which gives flexibility. Moreover, they have ease of manufacturing and low production costs [20-21].

Perovskite solar cells (PSCs) are devices that can achieve high efficiencies. Moreover, the manufacturing process is easy, at low temperature and with low cost. However, they are very unstable, they degrade in short periods of time and their toxicity can be dangerous in the fabrication process. In photovoltaics, this form of solar cell is predicted to be the leader as we can see with its evolution during the years in figure 1.7 [22].

Organic Photovoltaics (OPVs) solar cells used various absorbers to create coloured or transparent devices. The main benefit is that they use flexible substrates that allow a wide variety of uses [23].

Quantum dot-sensitized solar cells (QDSSCs) have appeared after the research on the aforementioned dye-sensitized solar cells progressed. Quantum dots is the material used as an absorber. It is made of nano-dimensional structures with a narrow band-gap suitable for absorbing light in the visible region [21].

In this group of research and development photovoltaic technologies, there are also solar cells called multi-junction (MJSC) that are formed by using different materials to obtain several p-n junctions. As these are the types of cells that are going to be studied during this document, they are going to be explained deeply in the next chapter.

1.2 Project motivation

As it was mentioned at the beginning of this chapter, the current energy model based on fossil fuels has collapsed. For this reason, to achieve the transition goals to reach a sustainable environment, the investigation in the development of solar cell technologies plays a very important role.

Generally, there are two main focal points in the research and expansion of photovoltaic cells that are, increasing the cell's efficiency and reducing the production cost. Currently there are different techniques to characterize solar cells with the aim of evaluating several parameters to find the ideal materials to use.

To measure and analyse the efficiency of solar cells there are different techniques but the most used are the following: Maximum Power Point Tracking (MPPT) method, that consists of measuring the maximum power that the generator can produce for the atmospheric conditions in every specific moment, analysing some operating parameters that are going to be explained in the next chapter, and Quantum Efficiency (QE) that will be the procedure used in this investigation using a spectral response characterization equipment, developed in more detail throughout this document.

The motivation of this project is to start a photovoltaic characterization equipment in the UC3M Physics Department to be able to characterize different types of last generation photovoltaic devices. The line of research of this project is to continue using this equipment as a quality control tool of different technologies to improve the manufacturing process and thereby create more efficient cells that can be competitive with the traditional silicon-based cells.

1.3 Goals

During the development of the presented project in this document, the following objectives have been set:

- Acquire the knowledge of the different techniques used for the characterization of photovoltaic solar cells.
- Gain an understanding of the standard conditions needed for doing the correct measurement of a solar cell so that all the obtained results are taken under the same conditions.
- Put into operation a spectral response characterization equipment in the Physics Department of Universidad Carlos III de Madrid for a research line on solar cells.
- Be aware of the limitations of the equipment mentioned just above.
- Understand the existing dependence between the gap of the materials and its quantum efficiency through the analysis of solar cells based on different materials.
- Study the effect caused by the modifications of some modular parameters (such as doping concentration, minority carrier lifetimes, thickness) in the quantum efficiency of the solar cells.

1.4 Structure of the project

In order to accomplish the above-mentioned goals, the thesis have been divided into five chapters, organised in the following way:

The **first chapter**, already exposed, is a brief introduction, including an explanation of the complex situation that the actual energy model is suffering, augmenting the need for renewable energies, such as photovoltaic solar cells. It also includes the evolution of solar cell manufacturing technologies across the past years.

In the **second chapter**, it is explained the working principle of a solar cell, how they profit from the solar spectrum, and the possibilities to obtain photovoltaic devices with higher efficiencies. For example, by combining different materials on the same solar cells, the range of wavelengths that the solar cell absorbs to convert it into electricity can be greatly increased. This conclusion leads us to the use of multi-junction solar cells, the type of cells that will be studied during this project. Therefore, the structure, functioning and operating parameters of this photovoltaic technology will be also introduced so that we can analyse the results obtained in the photovoltaic characterization of the already mentioned multi-junction cells.

To understand the steps which must be followed to achieve the goals of this final thesis, we need to study the selected technique to characterize the cells that are the spectral response in a deeper way, so that we can understand the measuring principle. For this reason, it is exposed the functioning of the I-V curve, the spectral response and the quantum efficiency.

Once all these basic principles have been explained, it will be introduced in the **third chapter** the specific concepts of this study: the reference cell used to calibrate the spectral response equipment, the three different multi-junction solar cells that are going to be analysed with the spectral response characterization equipment in the Physics UC3M Department, and the description of all the apparatus that composes this equipment with the corresponding explanation of its working principle.

In the **fourth chapter**, it is studied the effect of the materials band-gap on the quantum efficiency. The measurement obtained from the reference cell explained in the previous chapter is analysed, and once we have this, the project will continue with the analysis of the three III-V multi-junction cells.

To complement this investigation, the effect caused by modifying the modular parameters of the photovoltaic devices in the external quantum efficiency is exposed. This analysis is established by using some Python simulations.

Once all the laboratory and simulation results are obtained, we will finally study in the **fifth chapter** whether or not the already exposed goals have been achieved. In case they are not, the reasons for it will be studied.

CHAPTER 2
SOLAR CELLS

2. SOLAR CELLS

2.1 Theoretical fundaments

As it was already mentioned in the previous chapter, a photovoltaic cell, also known as solar cell, is an electronic device which directly converts sunlight (solar energy) into useful electricity. The exposition of the cell to photons (particles of light), produces current and voltage to generate electric power by the process called photovoltaic effect.

One of the most important things that are required to develop this method are the used materials, in which the absorption of light raises an electron to a higher energy state. This effect can occur in solids, liquids and gases, but nowadays the best efficiencies are achieved in solids [24-25].

There exist a wide range of types of PV cells, the vast majority of them are made by semiconductor materials, as their atoms are very sensitive to the energy photons of the solar radiation, so these materials interact with the incoming photons from the Sun and with the movement of electrons they are able to generate an electric current.

During 1940 and 1950 the study of those semiconductor materials increased and thanks to that they obtained a more solid general view of semiconductors, reaching an explanation of how the electrons are moved through the energy levels.

In semiconductors we can mainly have electrons in two energy bands that are represented in figure 2.1: the valence band, representing the energy level where the electrons in the last orbital are located, and the conduction band, in which the electrons that already broke their bond with the atom are, moving freely and participating in the conduction. Both bands are separated by the band-gap (Eg) that represents the minimum energy needed for an electron to break the bond with the atom and jump to the conduction band.

The reason why semiconductor materials are used instead of insulators for solar devices is because of the distance between the valence band and the conduction band, there is a huge difference in the band-gaps. In an insulator it is too large, making it difficult for electrons to jump into the conduction band, a lot of energy is needed to become a free electron. However, semiconductor band-gaps are smaller, and it is easier for the electrons to move from the valence band to the conduction one. As an example, at a temperature of 300 K, for semiconductors we have Silicon (Si) with a band-gap of 1.12 eV and Gallium arsenide (GaAs) with a band-gap of 1.43 eV, while for insulators we can use as an example Magnesium oxide (MgO) has a band-gap around 7.5 eV [26].

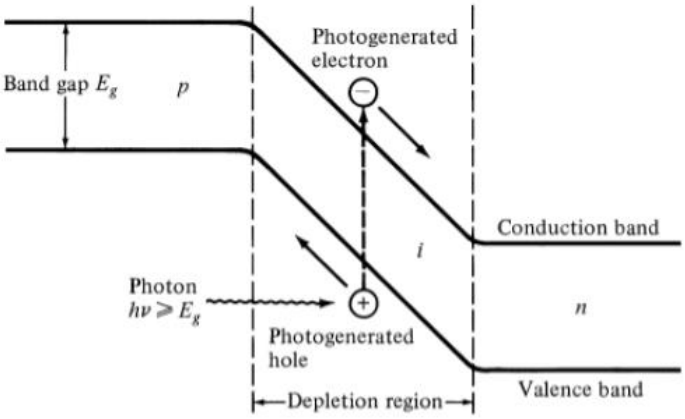

Figure 2.1 ENERGY BAND DIAGRAM INDICATING THE PHOTOGENERATION PROCESSES [27].

Because of the fact that was just stated, the electrons used to generate electric current are the ones in the last orbital, the valence electrons, because as they are far from the nucleus which is attracting them it is easier to move them to the conduction band [11].

2.1.1 P-n junction

Silicon (Si) is the most widely used material in photovoltaic systems. Silicon atom has 14 electrons, but only the outer four of these, the valence electrons, can move between other atoms and enter into chemical reactions.

The intrinsic carrier, that is the electrons and holes that are in the conduction band and therefore participate in conduction, depend on the temperature and the band-gap of the material. In silicon at normal temperature (25 ºC) the intrinsic carrier density is really low, around 10^{10} cm^{-3}, which means that the conductivity of the material is very low. That is the reason why to create a semiconductor device, the semiconductor material is doped by the addition of impurities, so that the quantity of electrons and holes is increased and by this way the conductivity of the material.

An n-type semiconductor is an intrinsic semiconductor, in which a donor impurity has been purposely introduced. The impurities in this case are called donors because after the rearrangement of elements there is a remaining electron that will rotate as a mobile negative charge in the conduction band around the positively charged impurity atom.

As it is seen in figure 2.2, in an n-type material the free electrons are in the top of the band-gap, close to the conduction band so that they can be easily excited and jump into the conduction band [28].

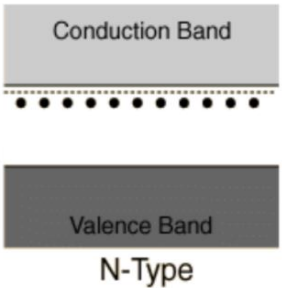

Figure 2.2 N-TYPE SEMICONDUCTORS [28].

In p-type semiconductors the added impurity is called acceptor, because when they are inserted in the crystalline lattice, a hole appears in one of the bonds to the impurity. Once this hole is created the same process as in n-type is happening but, in this case, the moving elements are the holes. After the completion of the initial hole, the impurity, now negatively charged, will attract the positive and by this way is moving and contributes to the conductivity.

The addition of acceptor impurities creates holes next to the valence band as it is depicted in the below image. The presence of these holes attracted electrons from the valence band to them and by this way the moving process starts [28].

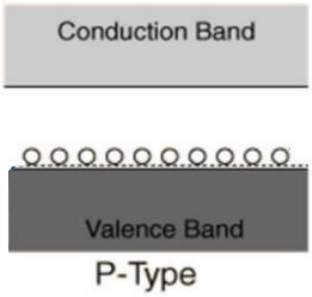

Figure 2.3 P-TYPE SEMICONDUCTORS [28].

When both materials (n-type and p-type) are put together as it happens in PV cells, a current of holes is created that moves in the direction of n-region and in the opposite way, a current of electrons is created from n-region to p-region.

The zone that is the border between the n-type and p-type material is called p-n junction. In this junction, there are no holes or electrons but because of the currents created by them, there are ions with opposite sign in each boundary, which causes the presence of a permanent electric field that goes from the positive charge region to the negative charge region as it is represented in figure 2.4, and therefore a potential difference is created [29].

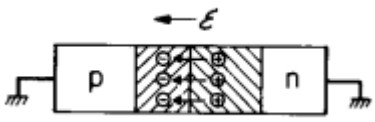

Figure 2.4 ELECTRIC FIELD CREATED BY THE IONS WITH OPPOSITE SIGN [29].

2.1.2 Working principle

As it was introduced in section 2.1, solar cells are made by semiconductors that are doped with two different materials, one with positive charge and the other with negative charge. When the sunlight hits the surface of the panel that is connected to an external load, and the photons have a higher energy than the band-gap, electrons are taken off from the material and leave a hole that will be replaced by another electron to which the same happens, like a chain process, electron-hole pairs are created. The movement of the electrons from the positive terminal to the negative produces an electric current and a potential difference.

This process is represented in the following scheme 2.5, where it is possible to see the internal movement of the electrons and holes in the cell and also in the external circuit through the load [11].

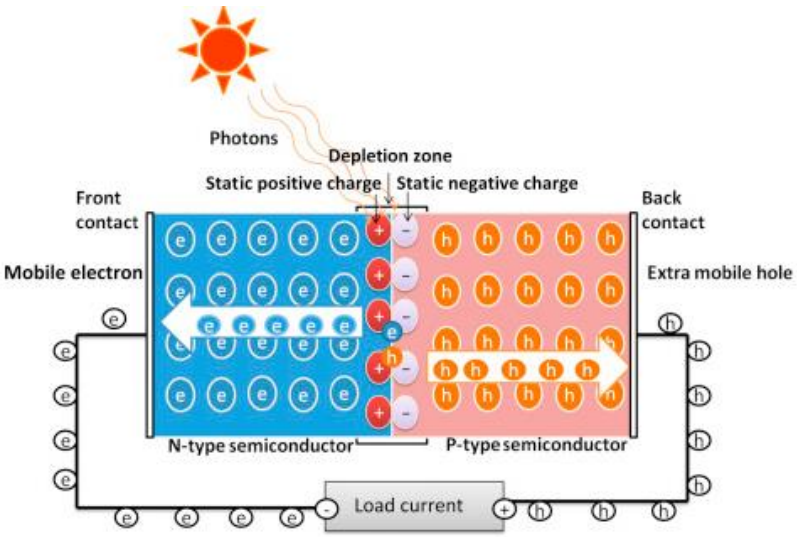

Figure 2.5 SCHEMATIC REPRESENTATION OF HOW A PV CELL WORKS [30].

2.2 Solar spectrum

The sun is the closest star to the earth, and is a hot gaseous sphere composed mainly of hydrogen. This structure of this body is divided into different layers. Starting from the inside we have the core and the interior that are compared to a nuclear reactor because they are the hottest parts where temperatures of 20,000,000 K can be reached and are the origin of nearly all sun's energy. However, the solar radiation that reaches the earth in the form of electromagnetic waves came from the surface of the sun, called photosphere, that emits a radiation that is approximated to the one that would emit a black body at 5,777 K [31].

This radiation emitted from the sun is more or less constant but when arrives to the earth's surface, it starts to be altered by the atmosphere constituents, mainly because of two

processes, the atmospheric absorption by O_3, H_2O and CO_2 and the dispersion or scattering when solar radiation interact with water vapour, air molecules and pollution that is present in the atmosphere [32].

Within the scattering in this case, we can differentiate between two types that are Rayleigh and Mie. Rayleigh scattering is caused by the air molecules that are present in the atmosphere and occurs at short wavelengths because the molecules are really small. On the other hand, Mie scattering befall because of pollution. In these cases, if the size of the particles is smaller than the wavelength, the light is separated and it is scattered in all the wavelengths that compose it, but, on the contrary, if the sizes are bigger and that condition is not fulfilled, the light will stay the same and we will see the same colour.

The efficiency of the solar cells is affected by the changes in two variables: the irradiance and the solar spectrum. Mainly we can state that there are two variables that have to be taken into consideration when analysing the solar spectrum: the spectral irradiance and the Air Mass, that is related to the angle of incidence [33].

The irradiance is the power of the solar radiation per unit area (W/m^2), the energy from the sun that hits a square meter of earth, and it is all the time changing, depends on the distance between the sun and the earth, the angle of declination, the time of the day, the latitude of the place where impact, etc. [34]. Moreover, we have a way of characterising a light source that is by using the spectral irradiance, that is similar to the solar irradiance but as a function of the wavelength of the arriving photon, so it is the radiant flux of wavelength per unit area of the surface where it arrives, and its units are $W/m^2 \cdot \mu m$ (irradiance units and the wavelength) [35-36].

In order to facilitate the calculation of the solar radiation reaching a horizontal surface on the earth, a reference line called zenith or observer's zenith that is normal (90º) to the earth's surface at the observer's position is used. By means of this line, we have the zenith angle (θ) (also called zenith distance) that measures the angle between the zenith line and the line joining the observer and the sun. These parameters can be represented in figure 2.6 where it is also included the other factor that it was mentioned before, the Air Mass, that is an element completely necessary to compare different solar cells, with different characteristics and locations [31].

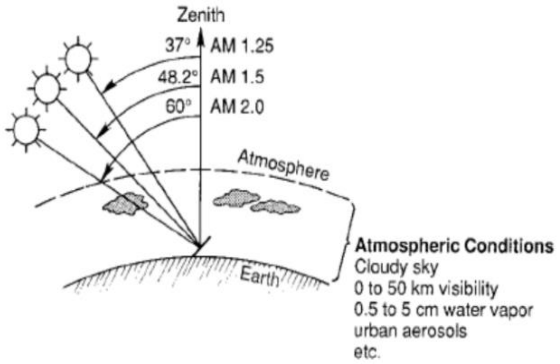

Figure 2.6 ZENITH ANGLE FOR DIFFERENT VALUES OF AIR MASS [34].

Fixing a reference spectrum allows us to do all the measures (industry, scientific community, etc..) using the same situation, performed in the same conditions and therefore are comparable and objectively evaluated.

The ASTM (American Society for Testing and Materials) has developed three reference solar spectra (standards, ASTMG173-03 [53] and ASTME490 [54]), that considers the trajectory of the solar radiation:

- The Air Mass Zero (AM0) is when the incidence of the light is completely perpendicular, coincides with the zenith light so $\theta = 0^{o}$. It is called extra-terrestrial spectrum and is used by the aerospace community.
- The Air Mass 1.5 Direct (AM1.5D) represents the direct component of the spectrum (before entering into the atmosphere so that the constituents present do not affect it). It has an angle of $\theta = 48.2^{o}$ and is used in PV concentration.
- The Air Mass 1.5 Global (AM1.5G) takes the direct light component and the scattered light component (light that enters into the atmosphere). This last reference solar spectrum is the standard used in conventional photovoltaic cells. For AM1.5G it is considered a reference value of irradiance of 1000 W/m^2, as it is defined in international standard IEC 60904-3 [55].

All these three solar spectra are usually represented in the graph shown in figure 2.7.

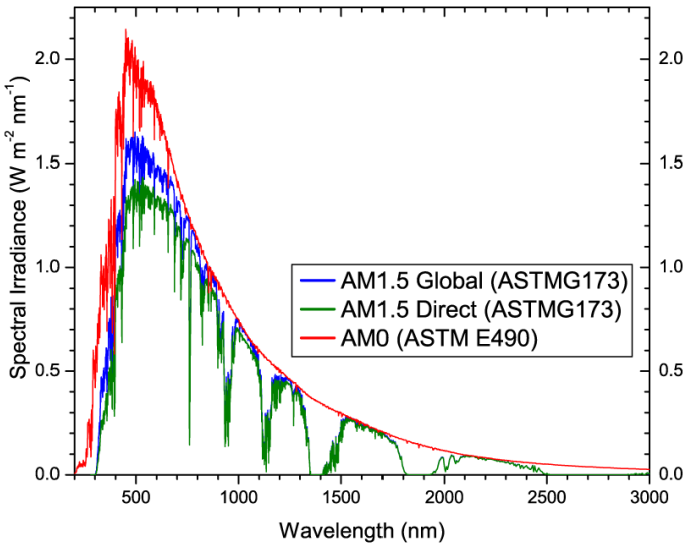

Figure 2.7 SPECTRAL DISTRIBUTION OF SOLAR RADIATION [37].

As it was mentioned and previously represented in figure 2.7 in blue, the AM1.5G, is the solar spectrum that considers all the light components that arrive at the Earth's surface. Although this entire solar spectrum reaches the photovoltaic cells, they are not capable of converting all of it into useful energy.

This can happen because the photons are reflected and directly do not enter the solar cell or because they reach the cell, but they are not absorbed, as the band-gap of the material does not correspond with the energy that these particles of light have.

As most of the solar cells in the market are made of silicon, we are going to take this type of cells as an example to see how much of the standard solar spectrum (AM1.5G) are able to use [37].

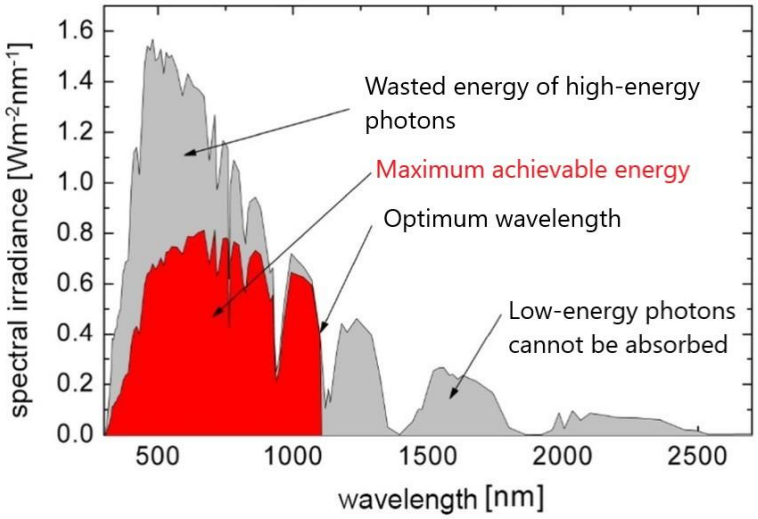

Figure 2.8 SOLAR SPECTRUM ABSORBED BY A SILICON CELL COMPARED WITH THE COMPLETE AM1.5G SOLAR SPECTRUM [38].

Here in figure 2.8, we have represented in grey the standard solar spectrum and in red the part of the spectrum that Si solar cells are capable of using. The left-side of the spectra corresponds to wavelengths lower than the energy band-gap (energies higher than the band-gap). Here there are some losses because the energy of the arriving photons is too high to be absorbed, higher than the band-gap, and traverses the semiconductor without being absorbed. On the other hand, the spectrum remaining on the right part of the graph is not used by the silicon cells because the energy is below the band-gap and the electrons cannot be excited and promoted to the conduction band.

Looking at this graph we can draw a conclusion, much of the solar spectrum is wasted using cells made by silicon, they have its limitations. That is why the use of other materials or the combination of several of them is investigated in order to make the most of the sunlight.

This is for example the case of multi-junction cells, which, although they have an electrical conversion method similar to that of silicon cells, are more efficient as they make better use of light energy from the sun by having different layers with more than one type of semiconductors.

2.3 III-V solar cells

2.3.1 Structure and working principle

Multi-junction solar cells (MJSCs) are formed by different p-n junctions; they are different solar cells connected in series that use some types of semiconductors. Each junction produces current at different wavelengths so each of them can transform a different part of the solar spectrum into electrical energy. Moreover, the efficiencies of these devices are higher because the photons absorbed are also higher.

Materials of III-V semiconductors have excellent properties and ranges of band-gaps to be implemented in these multi-junction solar cells, especially the ones with germanium [39].

These solar cells can be manufactured in two different ways that are called mechanical stacked and monolithic cells. In the mechanical stacked method, each layer is manufactured individually and after that are joined using metallic contacts, so each sub-cell has its own terminals. However, the monolithic way of doing the multi-junction cells is more sophisticated as all the different sub-cells made by different semiconductors, are grown on a single substrate and are united with tunnel diodes so that as a result we obtain a cell with two contacts, as in the case of silicon solar cells with a positive and a negative terminal [40].

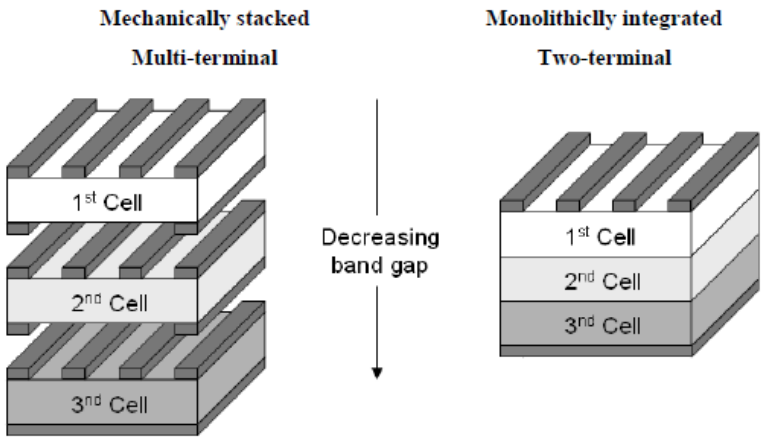

Figure 2.9 MECHANICALLY STACKED AND MONOLITHIC CELLS [40].

The cells are mainly divided in three regions: 1) the *window*, that is used to reduce the surface recombination[2] velocity at front surface and make it more sensitive to photons with higher energies, 2) the *emitter*, that is the layer closest to the top surface because its quality is better to absorb the photons from the solar radiation and it is formed by the n-

[2] Measure in cm/s of the rate of recombination between the electrons and holes at the surface of a semiconductor. [45]

type material; and 3) the *base*, that is just below the emitter and is made of p-type material. Between these two layers, where both meet, the p-n junction is created.

The order in which the different cell layers are located is determined by the band-gap of each material and its objective is to improve the fitting of the photovoltaic device to the solar spectrum. The top sub-cell is responsible for absorbing the photons with higher energy and allows lower energy photons to pass through it to be captured by the following sub-cells that have lower band-gaps. As it is represented in figure 2.10, the top sub-cell is the one in charge of taking the blue and green spectrum, the middle the red and orange spectrum and the last one absorbs the infrared spectrum [40].

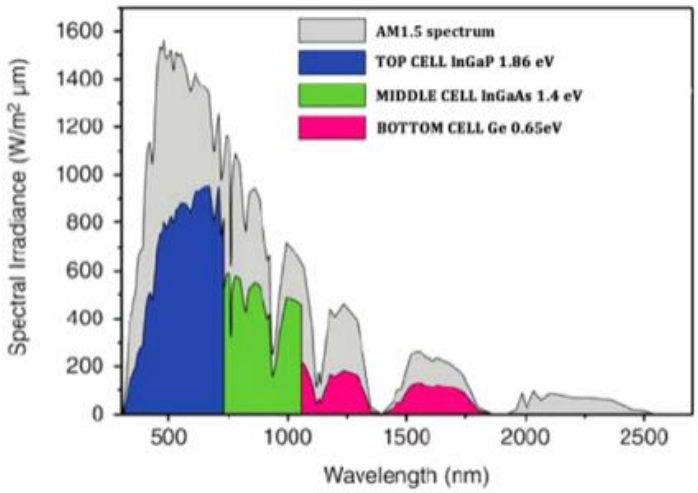

Figure 2.10 SOLAR SPECTRUM ABSORBED BY A MULTI-JUNCTION SOLAR CELL COMPARED WITH THE COMPLETE AM1.5G SOLAR SPECTRUM [41].

As stated at the beginning of this section, by adding different materials to form the cell, we are covering a wider range of wavelengths. We can use the case of a multi-junction solar cell that is represented here in figure 2.10 in which the sub-cells are covering all the coloured sections and compare it with figure 2.8 in which just a part of it was covered by the silicon.

2.3.2 Operating parameters

- **Characteristic Equation of a Solar Cell**

The equivalent circuit of a PV cell has a current source (Iv), a diode connected in anti-parallel (D), a series resistor (Rs) and a parallel resistor (Rp) as it is shown in figure 2.11.

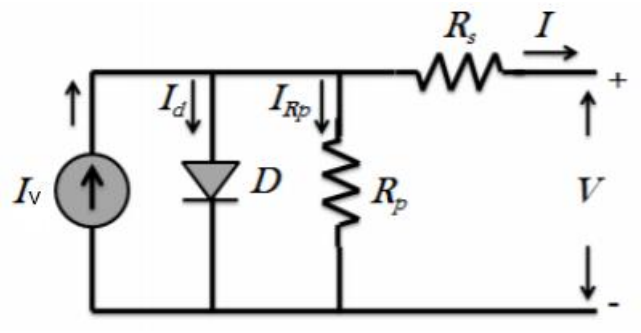

Figure 2.11 EQUIVALENT CIRCUIT OF A PHOTOVOLTAIC CELL [42].

When a solar cell is connected to an external load, it produces energy and depending on the conditions as to what it is exposed the values obtained for current and voltage vary.

Under Standard measurement conditions (Irradiance = 1000 W/m^2, AM1.5G spectrum and temperature = 25 °C) the equation to calculate the output current of the PV cell is an ideal one that is as follows:

$$I = I_L - I_D = I_L - I_O \cdot \left(\exp\left(\frac{q \cdot V}{m \cdot k \cdot T}\right) - 1\right) \quad (2.1)$$

Where I_L denotes light generated current, I_D is the current of the diode also named as dark current, I_O is the saturation current of the diode, q is the electron charge which is $1.60218 \cdot 10^{-19}$ C, m is the ideal factor of the cell and its values goes between 1 and 2 ($1 < m < 2$), k is Boltzmann constant ($1.38065 \cdot 10^{-23}$ J/K), and T is the absolute temperature [42].

A more developed equation considering all the elements that forms the photovoltaic cell as depicted in the equivalent circuit shown in figure 2.11 would be:

$$I = I_L - I_D = I_L - I_O \cdot \left(\exp\left(\frac{q \cdot V}{m \cdot k \cdot T}\right) + I \cdot R_S\right) - 1) - \frac{V + I \cdot Rs}{Rp} \quad (2.2)$$

The output voltage of the PV cell is expressed as:

$$V = (R_s \cdot I) - V_D \quad (2.3)$$

- **Short-circuit current**

The short-circuit current is the current that goes through the solar cell when the voltage across it is zero, when the solar cell is short-circuited.

I_L is the light generated current inside the solar cell but at short-circuit conditions the externally measured current is denoted as I_{SC}. Therefore, the photocurrent is:

$$I_{SC} \equiv I\,(V = 0) = I_L \tag{2.4}$$

The short-circuit current depends on a number of factors which are the following: the area of the solar cell, that we do not want to have so to remove this dependence on the solar cell area, it is more common to list the short-circuit current density (J_{sc} in mA/cm^2) rather than the short-circuit current; the number of photons, that corresponds to the power of the incident light source; the spectrum of the incident light; the optical properties (absorption and reflection); the collection probability of the solar cell, which depends chiefly on the surface passivation and the minority carrier lifetime in the base [42].

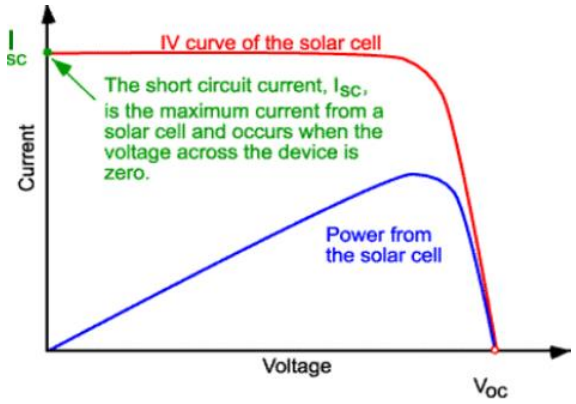

Figure 2.12 REPRESENTATION OF THE Isc IN THE I-V CURVE [42].

$$I_{SC} = q \cdot G \cdot (L_n + L_p) \tag{2.5}$$

Where G is the generation rate, L_n and L_p are the electron and hole diffusion lengths.

It is possible to obtain the IMPP (current at maximum power) by a linear relation with the I_{SC} of the photovoltaic system:

$$IMPP \approx k_2 \cdot I_{SC} \tag{2.6}$$

Where k_2 is a proportionality constant.

The measurement of the I_{SC} during the performance is problematic. For that reason, it is needed to add an additional switch to the converter to create the short-circuit periodically at the output of the installation [42].

- **Open-circuit voltage**

The open-circuit voltage, V_{OC}, is the maximum voltage available from a solar cell, and this occurs at zero current. The open-circuit voltage corresponds to the amount of forward bias on the solar cell due to the bias of the solar cell junction with the light-generated current [42].

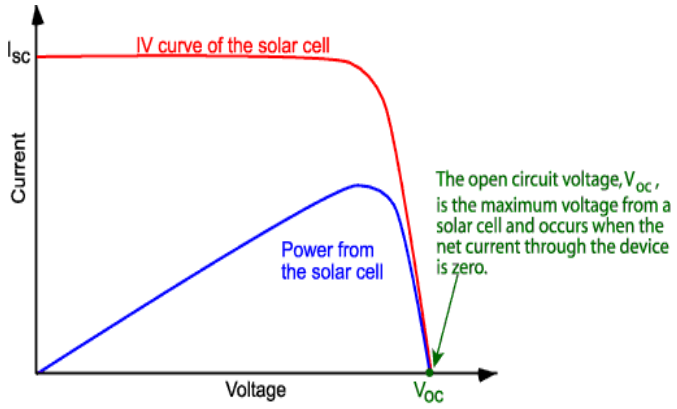

Figure 2.13 REPRESENTATION OF THE Voc IN THE I-V CURVE [42].

$$V_{OC} = \frac{m \cdot k \cdot T}{q} \cdot \ln\left(\frac{IL}{Io} + 1\right) \tag{2.7}$$

In the photovoltaic systems there exists a relationship more or less proportional between VMPP (voltage at maximum power point) and V_{OC} for different levels of temperature and irradiance.

$$VMPP \approx k_1 \cdot V_{OC} \tag{2.8}$$

Where k_1 is a constant and V_{OC} is calculated using the following formula:

VMPP can be calculated from the periodic measured values of V_{OC}. For that procedure it is needed to turn off the power converter [42].

- **Maximum Power Point**

The maximum power point is the product of the maximum point voltage (VMPP) and the maximum current point (IMPP) for which the power extracted from the photovoltaic array is also maximum (PMPP). This point changes mainly with the solar light intensity (irradiance) and the temperature but load variations can also affect it. It is important to work on this point because at the maximum power point (MPP), the PV operates at its highest efficiency.

There exist different tracking techniques to find the maximum power point that have been developed to use in the photovoltaic systems. The maximum power point trackers (MPPT) are electronic devices that get the photovoltaic generator to give in every moment the maximum power that the generator can generate for the atmospheric conditions in every specific moment [42].

The solar panel response can be analysed by using the I-V curve as it is shown in figure 2.14.

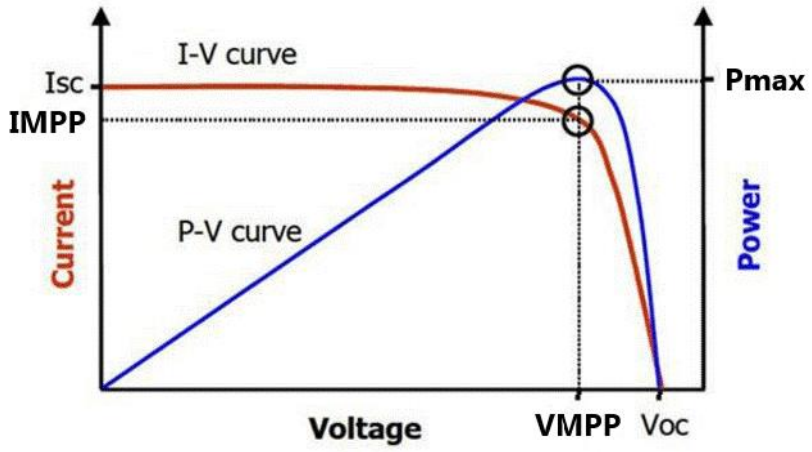

Figure 2.14 MAXIMUM POWER POINT REPRESENTATION USING I-V AND P-V CURVES [43].

No power is generated under short or open circuit. The maximum power (P_{max}) is reached at a point on characteristic where the product IV is maximum.

- **Fill factor**

The fill factor, commonly known by its abbreviation "FF", is a parameter related to the open-circuit and the short-circuit that determines the maximum power from a solar cell. The FF is defined as the ratio of the maximum power from the solar cell to the product of open-circuit voltage and short-circuit current. Graphically, the FF is a measure of the "squareness" of the solar cell and is also the area of the largest rectangle which will fit in the I-V curve [42].

$$FF = \frac{VMPP \cdot IMPP}{Voc \cdot Isc} \tag{2.9}$$

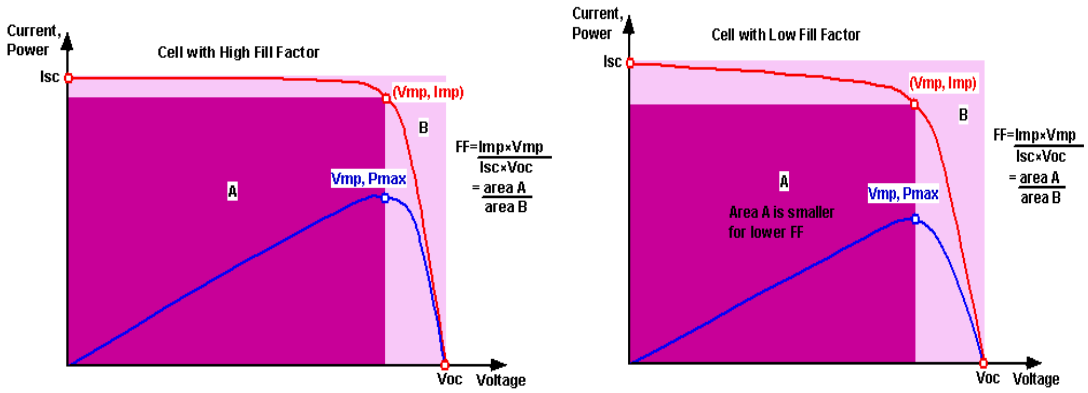

Figure 2.15 FILL FACTOR REPRESENTATION [42].

- **Efficiency**

The efficiency is defined as the ratio of the energy output from the solar cell to input energy from the sun. In addition to reflecting the performance of the PV cell itself, the efficiency depends on the spectrum and intensity of the incident sunlight and the temperature of the cell. Therefore, conditions under which efficiency is measured must be carefully controlled in order to compare the performance of one device to another. Terrestrial solar cells are measured under AM1.5G conditions and at a temperature of 25 °C [42].

The efficiency of a solar cell is determined as the fraction of incident power which is converted to electricity and is defined as:

$$P_{max} = V_{MPP} \cdot I_{MPP} = FF \cdot V_{OC} \cdot I_{SC} \qquad (2.10)$$

Once we have the maximum power calculated we can now introduce it in the efficiency formula stated below:

$$\eta = \frac{Pmax}{Pin} \qquad (2.11)$$

Here we have example of what would be the input power of a 10 x 10 cm^2 cell: 100 $mW/cm^2 \cdot 100\ cm^2 = 10$ W [42].

2.3.3 Photovoltaic characterization

- **I-V curve**

The characteristic curve of a PV panel is also called current-voltage curve, commonly known as I-V curve, represents the current and voltage values experimentally measured under different conditions of temperature and irradiance.

The I-V curve is used to see the performance of a PV cell or a PV module. The obtained graph from the device under test can be compared with a reference one, in which we know how the shape of the curve has to look like under Standard Test Conditions (STC) that are temperature of the cell equal to 25 ºC, solar irradiance of 1000 W/m^2 and Air Mass 1.5 G. With the shape of an I-V curve we can obtain a lot of information from the cell and detect if a cell is damaged, or it has any problem or potential issues in the future.

These standards are set by the International Electrotechnical Commission (IEC), which is a worldwide organization for standardization that has many different international standards for electrical and electronic fields, where there are also for PV energy systems. The IEC 60904-1 Standard [56] depicts the requirements for the measurement of photovoltaic current-voltage characteristics, such as irradiance and temperature. Another standard used for the I-V curve is the IEC 60904-10 [57] that describes the different methods of linearity measurement. And in IEC 60891 [58] Standard we can find the I–V curve temperature and irradiance correction [43].

The I-V curve that was already used in this document to represent in a graphical mode the operating parameters of the solar cell is represented as it is shown in the following figure 2.16, where the different parts are also remarked.

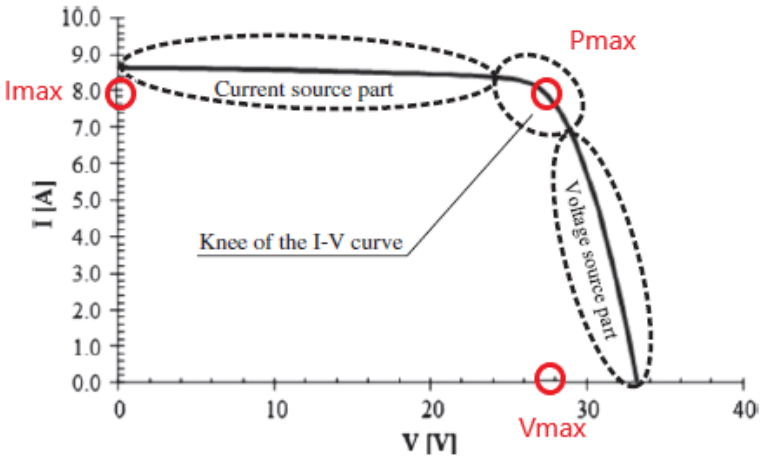

Figure 2.16 CHARACTERISTIC PARTS OF THE I-V CURVE OF A PV PANEL [44].

In the current source part, the voltage varies widely from 0 to V_{max} and the current is approximately constant. In the knee of the curve, we find the maximum power obtained (P_{max}) right in the corner part, going vertically to the x-axis we find the maximum voltage

(V_{max}) and going horizontally when it arrives the y-axis, we have the maximum current (I_{max}), representation already shown in figure 2.14. In the voltage source part, the current varies from 0 to Imax and the voltage is moving just a little bit from its initial point in this section [44].

Figures 2.17 and 2.18 are representing the effect of changes in temperature and irradiance in the performance of the cell, where i_{pv} and v_{pv} represent the output current and voltage of the cell.

We can see that these variations in the conditions under which the samples are analysed, affect the start and end points on the I-V curve while the trajectory of the line is similar between them.

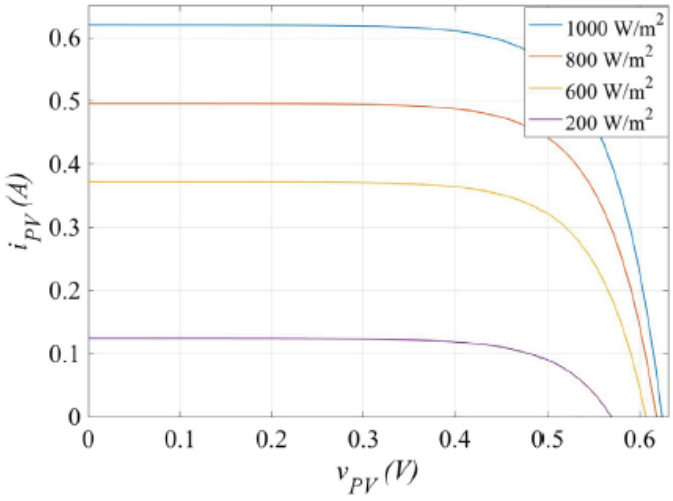

Figure 2.17 MODELLED I-V CURVE OF THE PV CELL WITH CONSTANT TEMPERATURE (25ºC) AND VARIABLE IRRADIANCE [43].

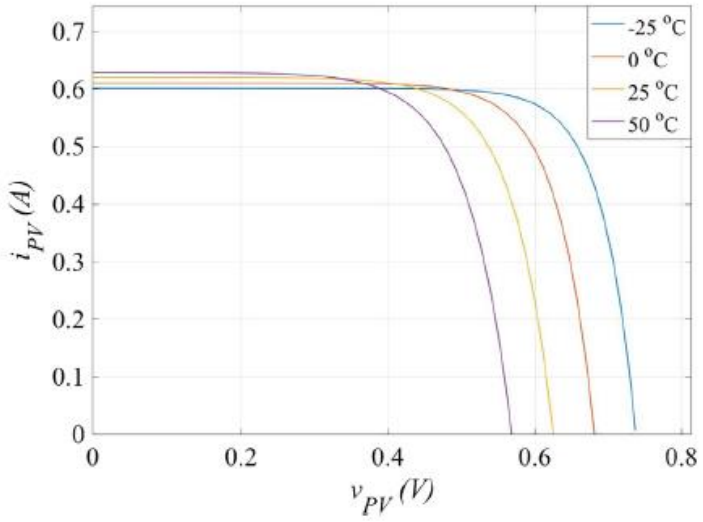

Figure 2.18 MODELLED I-V CURVE OF THE PV CELL WITH CONSTANT IRRADIANCE (1000 W/m2) AND VARIABLE TEMPERATURE [43].

- **Spectral Response and Quantum Efficiency**

For a certain wavelength, the spectral response of a solar cell is defined as the ratio between the photogenerated current and power of the incident radiation.

$$SR\ (\lambda) = \frac{I\ (\lambda)}{P\ (\lambda)} \tag{2.12}$$

An ideal solar cell generates current for each photon that reaches the solar cell and has greater energy than the band-gap and on the other way, generates nothing when the energy of the photons is less than the band-gap.

The maximum current generated by the cell is defined as:

$$I_{ideal}\ (\lambda) = q \cdot N_{ph}(\lambda) \tag{2.13}$$

Where q is the charge of the electrons and $N_{ph}\ (\lambda)$ is the number of photons for a certain wavelength.

The monochromatic light energy, light of a certain wavelength, is defined as:

$$E\ (\lambda) = h \cdot \upsilon = \frac{h \cdot c}{\lambda} \tag{2.14}$$

Where h is Planck's constant and υ is the frequency, which at the same time is the ratio between c, speed of light, and λ a certain wavelength.

The monochromatic light power is defined as:

$$P\ (\lambda) = N_{ph}\ (\lambda) \cdot E\ (\lambda) \tag{2.15}$$

Introducing formula 2.14 in formula 2.15 we have that the monochromatic light power is:

$$P\ (\lambda) = N_{ph}\ (\lambda) \cdot E\ (\lambda) = N_{ph}\ (\lambda) \cdot \frac{h \cdot c}{\lambda} \tag{2.16}$$

With all these definitions we can now develop more the formula of the spectral response, formula 2.12, using formulas 2.13 and 2.16:

$$SR_{ideal}\ (\lambda) = \frac{Iideal\ (\lambda)}{P\ (\lambda)} = \frac{q \cdot Nph\ (\lambda)}{Nph\ (\lambda) \cdot \frac{h \cdot c}{\lambda}} \rightarrow SR_{\ ideal}\ (\lambda) = \frac{q \cdot \lambda}{h \cdot c} \tag{2.17}$$

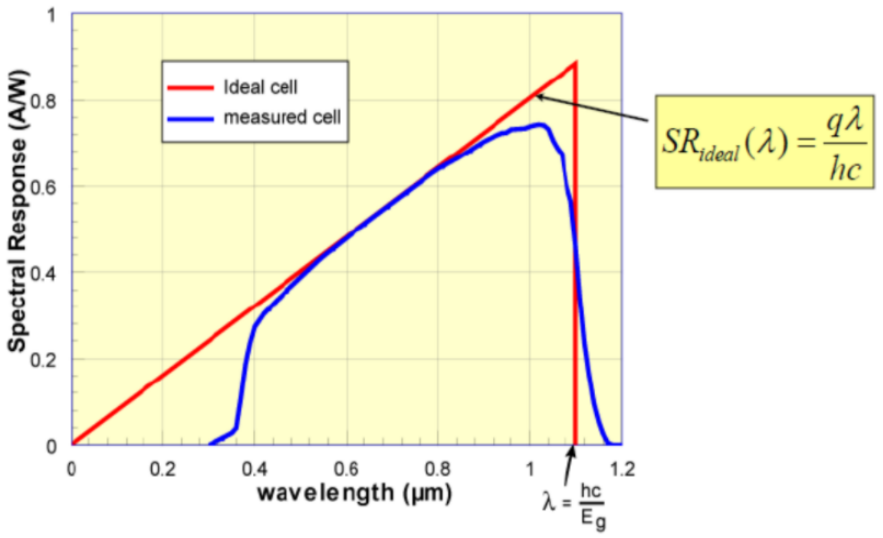

Figure 2.19 REPRESENTATION OF THE SPECTRAL RESPONSE OF AN IDEAL AND A REAL SOLAR CELL [37].

On the other hand, the quantum efficiency (QE) of a solar cell is the ratio between the number of electrons of the photogenerated current and the number of the incident radiation photons for a certain wavelength. It is the percentage of photons of a certain wavelength which end up contributing to the photogenerated current.

In an ideal solar cell, the quantum efficiency (QE) or external quantum efficiency (EQE) is equal to 1 if the wavelength is less or equal than the wavelengths accepted by the band-gap or 0 if the wavelength is higher than the gap, as it is represented in gold colour in figure 2.20 [37].

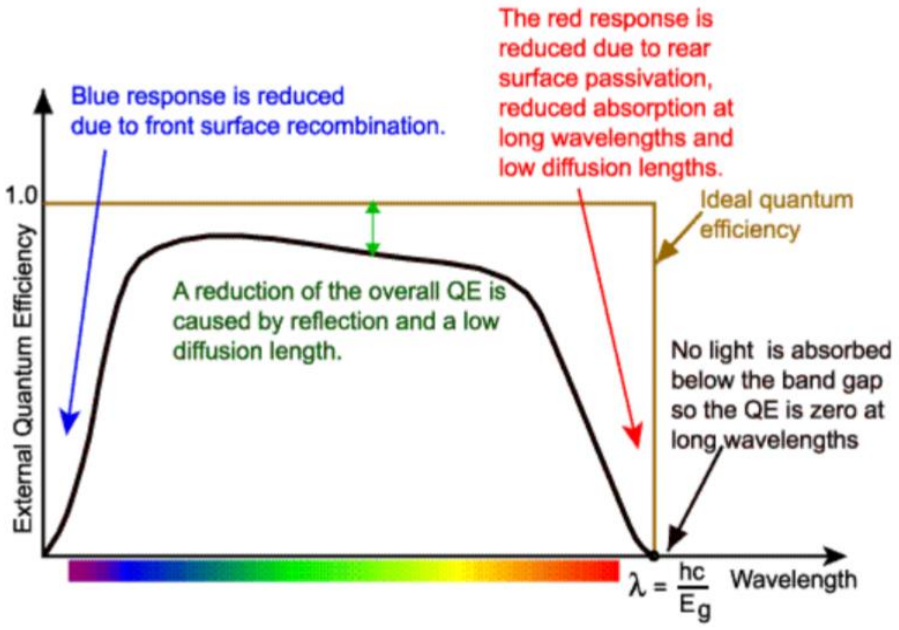

Figure 2.20 REPRESENTATION OF THE QUANTUM EFFICIENCY OF AN IDEAL AND A REAL SOLAR CELL [37].

Finally, the internal quantum efficiency (IQE) of a solar cell is the ratio between the number of electrons in the photogenerated current and the number of the incident radiation photons that penetrate the cell. It includes only material phenomena eliminating internal reflection losses, or in a simpler way: it is the percentage of photons of a certain wavelength which penetrate into the cell and end up contributing to the current photogenerated.

$$\text{IQE} = \frac{EQE}{1 - \text{R}} \tag{2.18}$$

Where EQE is the already defined quantum efficiency and R is the reflectance, the part of light that is reflected from the solar device.

Once we have defined all these terms, we can now expose the formula to calculate the real spectral response (SR), that is a different way to measure the same physical phenomena as the quantum efficiency (QE), as they are equivalent magnitudes [37].

If we expressed the quantum efficiency per unit, the relationship between SR and QE is the following:

$$\text{SR}(\lambda) = \frac{q \cdot \lambda}{\text{h} \cdot \text{c}} \cdot \text{QE}(\lambda) \tag{2.19}$$

To find the spectral response of a solar device, defined in the previous formula (2.19), the standard IEC 60904-8 [59] is used. This is a guideline of how to measure the spectral response of a photovoltaic device, with the characteristics needed to complete this procedure in the proper way. Measurements should be taken under the same temperature, so it has to be controlled all the time, and measurements of the short-circuit current and irradiance are also needed for each certain wavelength that we are selecting [34].

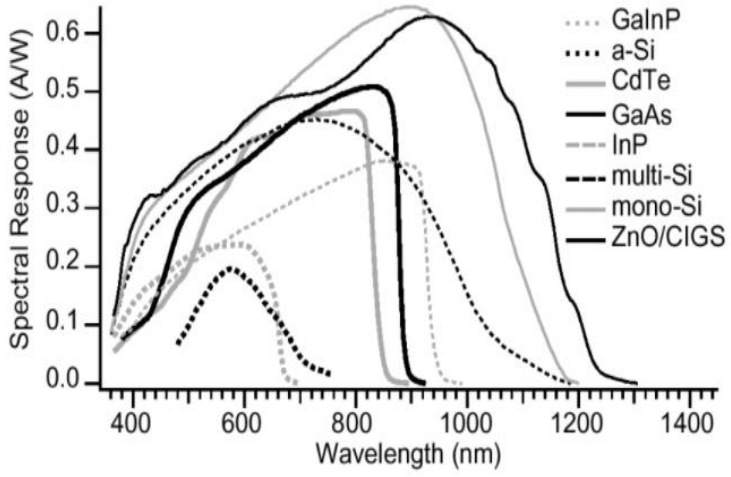

Figure 2.21 SPECTRAL RESPONSES FOR PV CELLS MADE BY DIFFERENT MATERIALS [11].

With the representation just above (figure 2.21), we can clearly see that depending on the materials used to manufacture the solar cells, different amounts of light will be captured. Reason why it is very important to continue in the research of new materials for the manufacturing of more efficient solar panels.

- **Calculation of the photocurrent**

In the last section of this chapter, it was described quantum efficiency and the spectral response. The relationship between the spectral distribution of solar irradiance and energy generation was also proven. Using this knowledge, we can assure that by having the information of the spectral irradiance and the spectral response of the studied device, we can obtain the photocurrent produced, as the spectral response is the basic analytical tool for calculating the photocurrent by using the following formula:

$$I_L = A \cdot \int_0^{\infty} E(\lambda) \cdot SR(\lambda)\, d\lambda \qquad (2.20)$$

Where A is the area of the solar cell, E(λ) is the monochromatic light energy (formula 2.14), and SR(λ) is the spectral response of the device (formula 2.19) [37].

CHAPTER 3
EXPERIMENTAL

3. EXPERIMENTAL

Once all the basic principles have been explained in the previous chapters, the introduction of the specific concepts of this study begins, including the information of the reference cell used to calibrate the spectral response equipment, the three multi-junction solar cells under test in the spectral response characterization equipment, and the description of all the devices that integrate this tool with the corresponding explanation of its working principle. Moreover, to complement this investigation, the theoretically effect caused by modifying some modular parameters in the quantum efficiency of a GaAs solar cell is exposed. This part of the project is done by using a Python code that provides the simulations shown in the results of the following chapter.

3.1 Analysis of the material band-gap effect on the quantum efficiency

3.1.1 Measuring set-up

The measurement of the external quantum efficiency is carried out by means of the spectral response equipment (as explained in section 2.3.3), represented in a schematic way in figure 3.2.

Figure 3.1 PARTS OF THE MEASURING EQUIPMENT.

The spectral response measurement equipment shown in figure 3.1 is comprised by the following numbered elements:

1. Newport Tunable Light Source (model TLS130B-250Q). Compact, fully assembled illuminator, that is composed by the following elements:
    a. Lamp (type QTH). The lamp produces a continuous and uniformly spectrum with a wattage of 250 W and a current of 11 A.

b. Wheel of filters. The filters have three positions to accomplish the whole range of wavelengths.
c. Monochromator (model CS130B). Device controlled by the computer that is used to select the working wavelength between the available tunable range that is 350-1800 nm. At the output, there is space to introduce slits to regulate the size of the spot of light.

2. Chopper (model SR540). Rotative switch with slot blades that can rotate at different frequencies, from 4 Hz to 3.7 kHz.

3. Pre-amplifier (model SR570). Is an adjustable device that allows to increase the signal acquired in the tested solar cell to 1MHz (maximum bandwidth) and also allows conversion of current into voltage.

4. Lock-in amplifier. Amplifier synchronised with the chopper whereby only the desired signal is detected.

5. Computer. Using TracQ BASIC Spectroscopy Control software the system can be remotely controlled.

The working principle of this technique is as follows: the light from the lamp (which tries to reproduce the solar spectrum), that is connected to a power supply, is passed through a monochromator where the wavelength is selected, using a computer, in between the different available wavelengths in a wheel of filters so that the light that hits the device tested is monochromatic.

Afterwards, the light from the lamp passes through a chopper, that is a rotary switch of light that is set at a selected frequency, different from the network to remove all the noise, so that by this way the signals can be measured in an accurate way reducing the errors. With the same aim, the chopper is connected and synchronised with a lock-in amplifier that allows it to select the frequency at which the chopper is rotating, reducing the noise and converting current into voltage.

Subsequently, the light reaches the device under test (DUT). This is connected to a pre-amplifier to increase that signal obtained by the illuminated cell which in turn, is connected to the aforementioned lock-in, where we obtained the generated voltage.

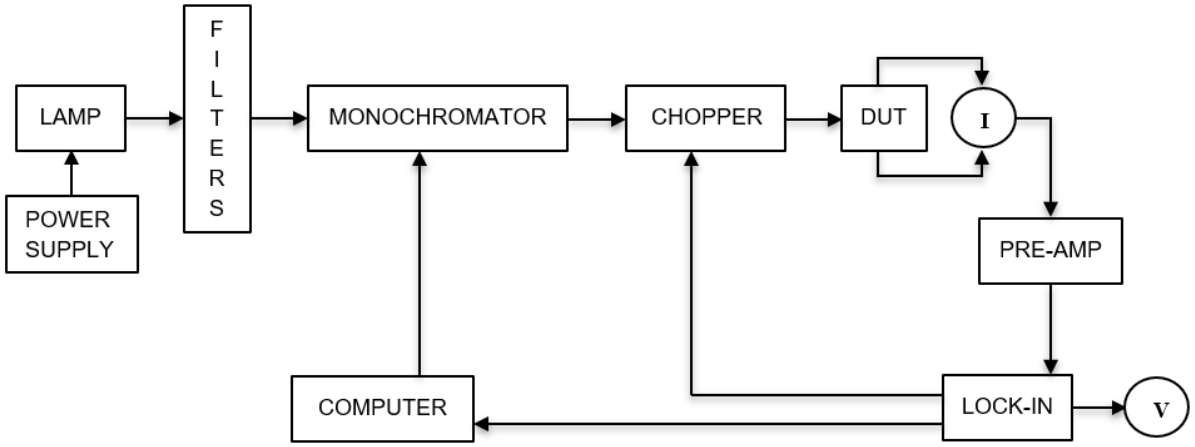

Figure 3.2 SCHEME OF THE SPECTRAL RESPONSE MEAUSREMENT EQUIPMENT.

3.1.2 Calibration and measurement procedure

As it was previously mentioned, the spectral response equipment needs to be calibrated before measuring any DUT.

The spectral response (SR) equipment measures current per unit of power [A/W]. However, from the equipment we extract voltage values [V]. Voltage and current are related by means of resistance as stated in Ohm's Law ($V = I \cdot R$). Therefore, contrasting the values measured in our reference cell (V_ref) with the known SR values of our reference cell (SR_ref), we can easily obtain the correction coefficient of our equipment.

This correction coefficient takes into account all resistive losses, including all the cables, from the system in that exact moment, and also the real power values per wavelength. Therefore, it is essential to carry out this calibration process before each measurement.

The calibration procedure is as follows:

- A reference cell is measured in the spectral response equipment obtaining voltage versus wavelength. Obtaining V_ref.
- The known (given by IES-UPM) values of the spectral response of the reference cell are recorded. Obtaining SR_ref.
- The correction coefficient is calculated using Ohm's Law (R = V/I) as following:

$$R = \frac{V\_ref}{SR\_ref} \tag{3.1}$$

Ongoing with the reference cell, once we have SR_ref, we can now calculate EQE_ref using formula 2.19:

$$EQE\_ref = \frac{h \cdot c}{q \cdot \lambda} \cdot SR\_ref \tag{3.2}$$

As soon as we have calculated the reference parameters and the correction coefficient of the equipment, we will proceed to measure our device under test (DUT) in the spectral response equipment, obtaining by this way V_DUT. Having R, calculated with the reference cell, and V_DUT, we can then calculate the spectral response of the DUT using formula 3.1.

$SR\_DUT = \frac{V\_DUT}{R}$, being $R = \frac{V\_ref}{SR\_ref}$, then:

$$SR\_DUT = \frac{V\_DUT \cdot SR\_ref}{V\_ref} \tag{3.3}$$

Following the same procedure as for the EQE in the reference cell, we can now calculate the EQE in the DUT:

$EQE\_DUT = \frac{h \cdot c}{q \cdot \lambda} \cdot SR\_DUT$, introducing SR_DUT from formula 3.3, we have:

$EQE\_DUT = \frac{h \cdot c}{q \cdot \lambda} \cdot \frac{V\_DUT \cdot SR\_ref}{V\_ref}$, and then introducing EQE_ref from formula 3.2, then we get the final formula to calculate the external quantum efficiency of the devices under test:

$$EQE\_DUT = \frac{V\_DUT \cdot EQE\_ref}{V\_ref} \tag{3.4}$$

It is important that measurements are always made with the same active area since the spectral response is measured per unit of power. If the spot is entirely inside the cell, no problems will be found. On the other hand, if it only illuminates one region of the cell, then it will need to be corrected.

3.1.3 Solar cells devices under study

In this project we are going to initially measure a reference cell and after that, some III-V semiconductor cells that will be introduced later in this chapter. The order of study of the cells is established in this way because it is essentially to have the equipment calibrated before starting with the III-V cell testing.

First of all, the measurement of a reference cell lent by the Solar Energy Institute of the Technical University of Madrid (IES-UPM) with the UC3M equipment will be done, and afterwards, these results will be compared with the ones obtained in the IES-UPM. With that we will be able to calibrate our equipment and get real measurements of the III-V solar cell as is going to be explained in section 4.1.1.

- **Reference cell**

A reference solar cell is a homogeneous silicon cell for which its spectral response under standard conditions is known. These solar cells are evaluated following the requirements for reference solar devices set in the international standard IEC 60904-2 [60]. They are calibrated under the reference conditions mentioned in the previous chapter, using an irradiance of 1000 W/m^2 as it is mentioned in IEC 60904-3 [55], and 25 ºC present in IEC 60904-1 [56]. Studying them in the laboratory under these conditions each reference cell has its own calibration report where all the operating parameters shown in section 2.3.2 are given and also includes the I-V curve [46].

In this study, the reference cell was borrowed from the Solar Energy Institute of the Technical University of Madrid (IES-UPM).

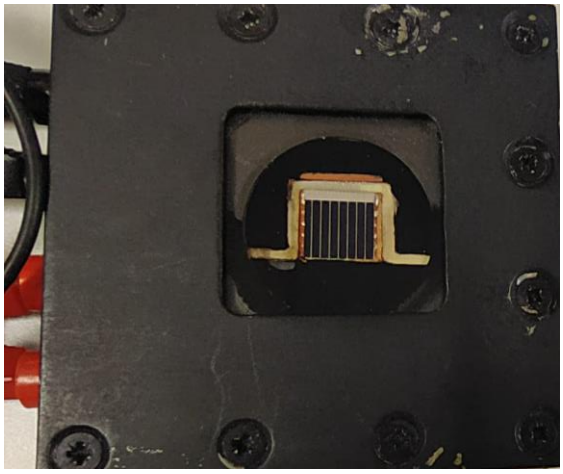

Figure 3.3 REFERENCE SOLAR CELL USED.

This cell shown in figure 3.3 is the one selected to use as reference in our experiments. The solar cell of 1 cm^2 area is made by monocrystalline silicon material and it is completely encapsulated in an aluminium box electrically insulated from the outside and mounted under BK7 glass. And it has 4 terminals, as shown at the left part of the image [47].

Table 3.1 OPERATING PARAMETERS OF THE REFERENCE CELL [47].

Parameters	Value
I_{SC}	30.5 mA
I_{MPP}	26.6 mA
V_{OC}	576 mV
V_{MPP}	45.7 mV
P_{max}	12.2 mW
FF	69.3%
η	12.2%

The operating parameters shown in table 3.1 are the ones obtained for our reference cell, that are reasonable lightning parameters, especially its I_{SC}.

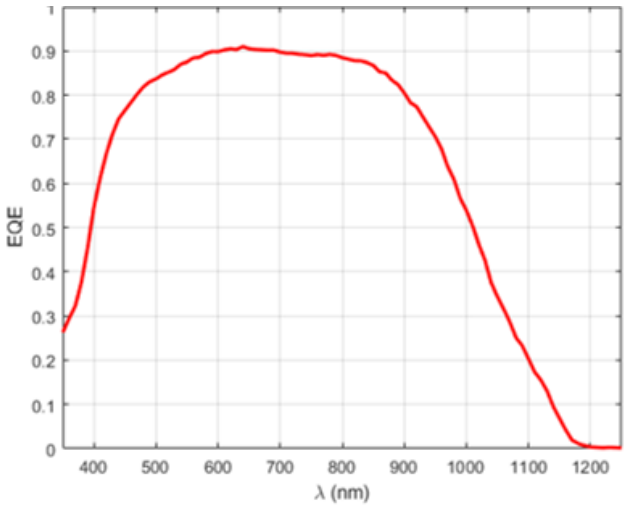

Figure 3.4 CALIBRATED EQE MEASUREMENT REPRESENTATION [47].

In figure 3.4 we have the final result of the EQE for our reference cell, calculated selecting a point for the spot of light in the middle of the cell.

- **III-V solar cells to be analysed**

The effect that the band-gap of the materials has on the spectral response of the cell is going to be analysed in this part of the bachelor thesis. To achieve that objective, three cells made by different III-V semiconductors are going to be under test.

- GaAs with a band-gap of 1.42 eV [48].
- GaInP with a band-gap of 1.87 eV [48].
- GaInAs composed by 25% of indium approximately, leading to a band-gap of 1 eV [48].

As the study of the dependence between the gap of the materials on its quantum efficiency is going to be developed and quantum efficiency is compared with wavelengths. The following equation is going to be used to convert the band-gap from electron volts to nanometres as photon energy is inversely proportional to wavelength:

$$E = \frac{h \cdot c}{\lambda} \tag{3.5}$$

Where h is Planck's constant ($6.6261 \cdot 10^{-34}$ J·s) and c is the speed of light ($2.9979 \cdot 10^{8}$ m/s).

The International System of Quantities (ISQ) have defined that 1 eV is equivalent to $1.60218 \cdot 10^{-19}$ J, then introducing the values written above, equation 3.1 would be as follows:

$$E\ (eV) = \frac{1239.8}{\lambda\ (nm)} \tag{3.6}$$

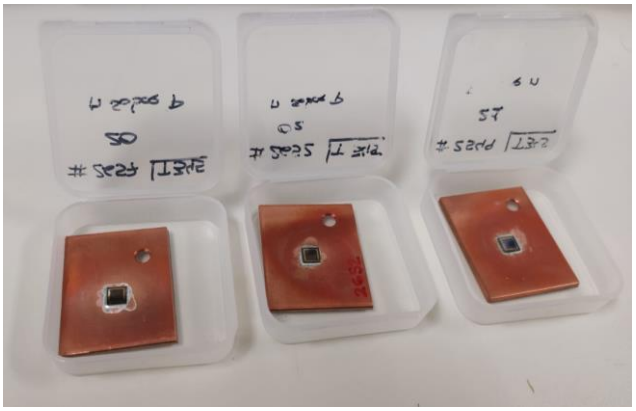

Figure 3.5 PHOTOGRAPHY OF THE GaAs, GaInP AND GaInAs CELLS UNDER STUDY.

The three cells shown in figure 3.5 are the ones that have been under test. They have been grown and processed at the IES-UPM laboratory, and they have lent them to us to start up our measurement system.

Spectral response must be measured in short-circuit. Therefore, it is necessary to get the contacts from the front and rear part of the cell to short-circuit them to afterwards connect them to the pre-amplifier.

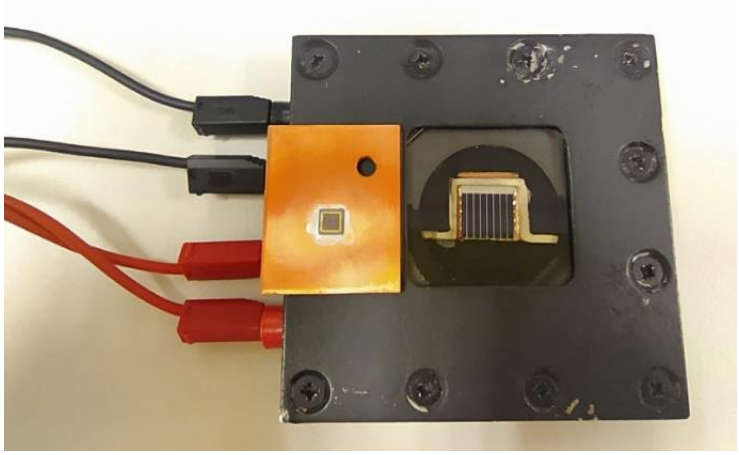

Figure 3.6 REFERENCE SOLAR CELL (WITH TERMINALS) AND III-V SOLAR CELL (WITHOUT).

As it is shown in figure 3.6, the reference cell (on the right) already has four terminals, red and black cables, that came from the front and back contact of the cell so it would simply be necessary to short-circuit these wires and measure the spectral response.

Nevertheless, the III-V cell (on the left) does not have terminals so the use of test probes will be required.

Furthermore, it can be seen in the above figure (3.6) the difference in size between the two types of cells. The reference cell is about 1.1 cm while the III-V cells are much smaller, with a size of around 5 mm.

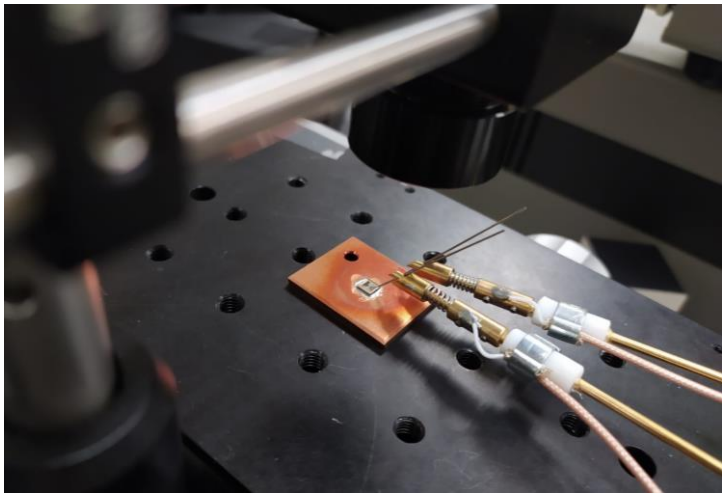

Figure 3.7 TESTED III-V SOLAR CELL MEASUREMENT USING TEST PROBES.

In figure 3.7 we can see the III-V cell with the test probes connected. One of them is connected directly to the cell (front contact) while the other has to be in contact with the copper platform (rear contact) where the cell is located. Once we have both contacts, the test probes have to be short-circuited.

3.2 Analysis of the material's properties effect on the quantum efficiency

3.2.1 Program used

This analysis of the photovoltaic device material's properties is done by using a code for modelling the quantum efficiencies of III-V solar cells that was developed in the UC3M Physics Department. Introducing the mentioned code in Python, gives the possibility to modify the studied parameters that are going to be explained in the following paragraph 3.2.2, and obtain the required simulations to do a deeper study and analyse them to obtain conclusions about what to adjust to obtain more efficient solar cells.

The code has been written using Hovel equations, that are used to calculate the quantum efficiency of a solar cell from several parameters (table 3.2). These equations are developed below [49].

$$QE_V = \frac{\frac{\alpha_V L_V}{(\alpha_V^2 L_V^2 - 1)}\left[\frac{\left(\frac{S_V\tau_V}{L_V} + \alpha_V L_V\right) - \exp(-\alpha_V W_V)\left(\frac{S_V\tau_V}{L_V}\cosh\frac{W_V}{L_V} + \operatorname{senh}\frac{W_V}{L_V}\right)}{\frac{S_V\tau_V}{L_V}\operatorname{senh}\frac{W_V}{L_V} + \cosh\frac{W_V}{L_V}} - \alpha_V L_V \exp(-\alpha_V W_V)\right]}{\frac{S_E\tau_E}{L_E}\operatorname{senh}\frac{W_E'}{L_E} + \cosh\frac{W_E'}{L_E}} \quad (3.7)$$

$$QE_E = \exp(-\alpha_V W_V)\frac{\alpha L_E}{(\alpha^2 L_E^2 - 1)}\left[\frac{\left(\frac{S_E\tau_E}{L_E} + \alpha L_E\right) - \exp(-\alpha W_E')\left(\frac{S_E\tau_E}{L_E}\cosh\frac{W_E'}{L_E} + \operatorname{senh}\frac{W_E'}{L_E}\right)}{\frac{S_E\tau_E}{L_E}\operatorname{senh}\frac{W_E'}{L_E} + \cosh\frac{W_E'}{L_E}} - \alpha L_E \exp(-\alpha W_E')\right] \quad (3.8)$$

$$QE_{zce} = \exp(-\alpha_V W_V - \alpha W_E')[1 - \exp(-\alpha W_{zce})] \quad (3.9), \text{ being} \quad W_{zce} = \sqrt{\frac{2\varepsilon V_{bi}}{q}\left[\frac{1}{N_E} + \frac{1}{N_B}\right]} \quad (3.10)$$

$$QE_B = \frac{\exp\left(-\alpha_V W_V - \alpha(W_E' + W_{zce})\right)\alpha L_B}{(\alpha^2 L_B^2 - 1)}\left[\alpha L_B - \frac{\frac{S_B\tau_B}{L_B}\left(\cosh\frac{W_B'}{L_B} - \exp(-\alpha L_B)\right) + \operatorname{senh}\frac{W_B'}{L_B} + \alpha L_B \exp(-\alpha W_B')}{\frac{S_B\tau_B}{L_B}\operatorname{senh}\frac{W_B'}{L_B} + \cosh\frac{W_B'}{L_B}}\right] \quad (3.11)$$

Table 3.2 PARAMETERS FROM HOVEL EQUATIONS [49].

Symbol	Meaning
q, X	Electron charge and level of luminous concentration
$N_f(E)$	Normalized photons flux per unit area and energy E
FS, R(E)	Shadow factor and spectral reflectivity of the structure
α_V, α	Window and GaAs absorption coefficient
L_V, L_E, L_B	Window, emitter and base diffusion length
τ_V, τ_E, τ_B	Window, emitter and base minority carrier lifetime
W_V, W'_E, W'_B, W_{zce}	Window, emitter, base and space charge zone (zce) thickness. In the emitter and base case, the area occupied by zce is removed
S_V, S_E, S_B	Window, emitter and base surface recombination velocity
N_E, N_B	Emitter and base doping, taking into account impurity compensation
ε	Semiconductor dielectric constant
V_{bi}	Voltage associated with the potential barrier height of the pn junction in equilibrium

3.2.2 Parameters to study

Among all the different parameters that exist in photovoltaic devices, the following parameters have been selected because they have the greatest impact on quantum efficiency as defined above in Hovel equations. Thus, greater variations can be seen in the Python simulations present in section 4.2.

- **Diffusion length**

The diffusion length is the average distance that an excited carrier will travel in a material before recombining. It is calculated using the following formula:

$$L_D = \sqrt{(D \cdot \tau)} \tag{3.12}$$

Where τ is the minority carrier lifetime and D is the diffusion coefficient, that is calculated following this Einstein relation:

$$D = \frac{\mu \cdot kb \cdot T}{q} \tag{3.13}$$

Where μ is the charge carrier mobility, k_b is the Boltzmann constant, T is the temperature, and q is the charge of an electron [50].

- **Minority carrier lifetime**

The minority carrier lifetime of a material is the average time which an excited carrier can spend before it recombines.

$$\tau = \frac{\triangle n}{R} \tag{3.14}$$

Where $\triangle n$ is the excess minority carrier concentration and R is the recombination velocity [51].

As shown in the above formulas and also in the definition of both parameters, diffusion length and minority carrier lifetime are related terms. Since they are linked, they vary together. If the diffusion length is high, it means that the minority carriers can travel long distances without recombining, so their lifetime is also high, and vice versa.

- **Surface recombination velocity**

When electrons are excited to higher energy levels, the electrons and holes can return to equilibrium by means of recombination at the surface. If the velocity is high, the electron hole pairs are formed before they can be used in the conversion process, the reason why recombination effects reduce quantum efficiency. Therefore, surface recombination velocity must be taken into account when developing the window layer of a solar cell. This parameter has to be reduced as much as possible to slow down the recombination process [52].

- **Thickness**

The thickness of the material that composes the different layers of the solar cell is a parameter that contributes to the changes in quantum efficiency, as the absorption of light is affected with the width of the layer.

Thicker solar cells can absorb more photons of light but will also experience higher recombination velocities, which can be a problem if the electrons and holes recombine before they are used. On the other hand, if the cell is very thin, it will absorb far fewer photons. Therefore, to achieve maximum efficiency of a solar cell the thickness has to be balanced with the surface recombination velocities.

CHAPTER 4
ANALYSIS OF THE RESULTS

4. ANALYSIS OF THE RESULTS

As it was introduced and theoretically described in the previous chapter, the effects of the materials band-gap on the quantum efficiency are studied. First, using a reference cell and once the measurement equipment is calibrated, the project will continue doing the same research but for the three III-V multi-junction solar cells that we want to study in more detail.

Moreover, in this fourth chapter is also studied the effect of the material's properties on the quantum efficiency to complement the previous analysis of the band-gap, trying to find with simulations in Python how to improve the efficiency of future solar devices. In this case it is going to evaluate the consequences of modifying the modular parameters of a GaAs cell.

4.1 Analysis of the material's band-gap effect on the quantum efficiency

4.1.1 Solar cells devices under study

- **Reference cell**

The Si reference cell was measured with the spectral response equipment at the UC3M laboratory. The obtained V_ref has been plotted in figure 4.1.

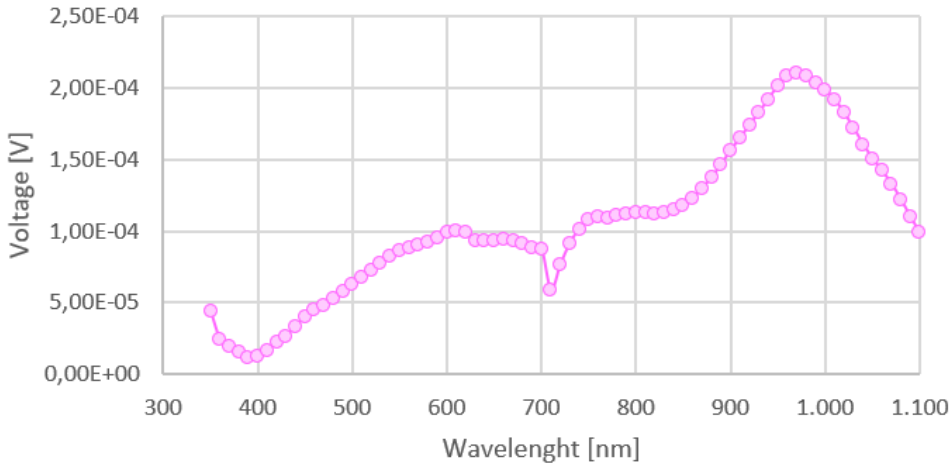

Figure 4.1 REFERENCE CELL CURVE (V_ref).

The peak between 700 and 730 nm is an artefact of the measurement related to the change of the filter. Nonetheless, the calibration process takes into account all these effects and corrects them on the final SR_DUT.

Taking the values of the reference cell V_ref represented in figure 4.1 and dividing it by the SR_ref (provided by the IES-UPM) it is possible to calculate the correction coefficient R as a function of wavelength following formula 3.1.

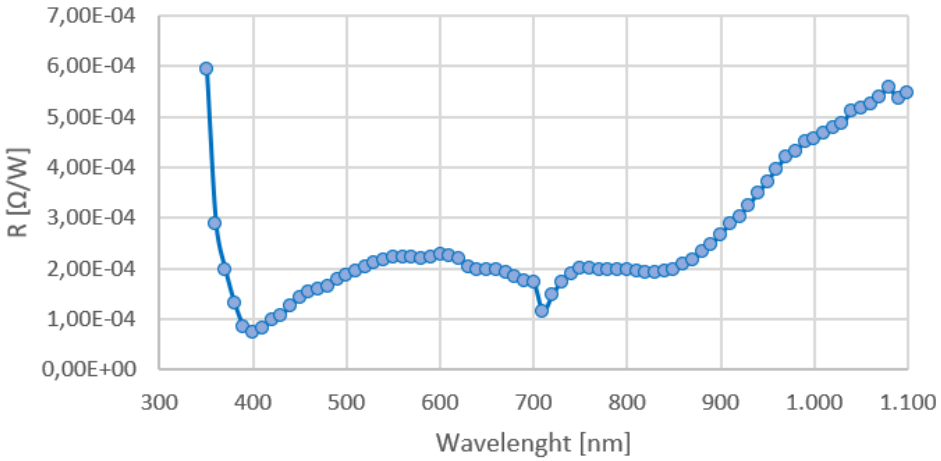

Figure 4.2 REPRESENTATION OF THE CORRECTION COEFFICIENT.

- **III-V solar cells to be analysed**

The three III-V solar cells that were introduced in chapter 3, were measured after the reference solar cell using the same equipment but, in this case, while the results were showing in the TracQ BASIC Spectroscopy Control software, we realized that they were not correct. Comparing the obtained results in the UC3M laboratory with those provided by IES-UPM, we confirmed that something was not working correctly in our spectral response equipment.

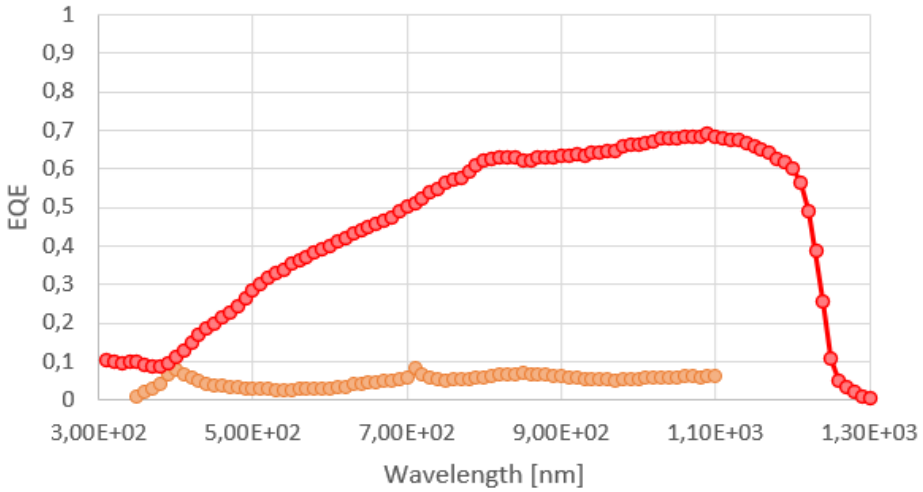

Figure 4.3 GaInAs EQE MEASURED IN THE UC3M LABORATORY VS. IES LABORATORY.

As an example, in figure 4.3 we can see the already mentioned comparison between the obtained EQE results in the UC3M laboratory (orange graph), transforming the spectral response obtained with our equipment into EQE using formula 3.4, and the data provided by IES-UPM (red graph). It is clearly seen that our results are not even close to reality.

After trying and testing different possibilities, we were finally unable to get a proper measurement with our equipment. Therefore, to continue with the research presented in this project, the data provided by IES-UPM is going to be used to analyse the dependence of quantum efficiency on the band-gap of the materials.

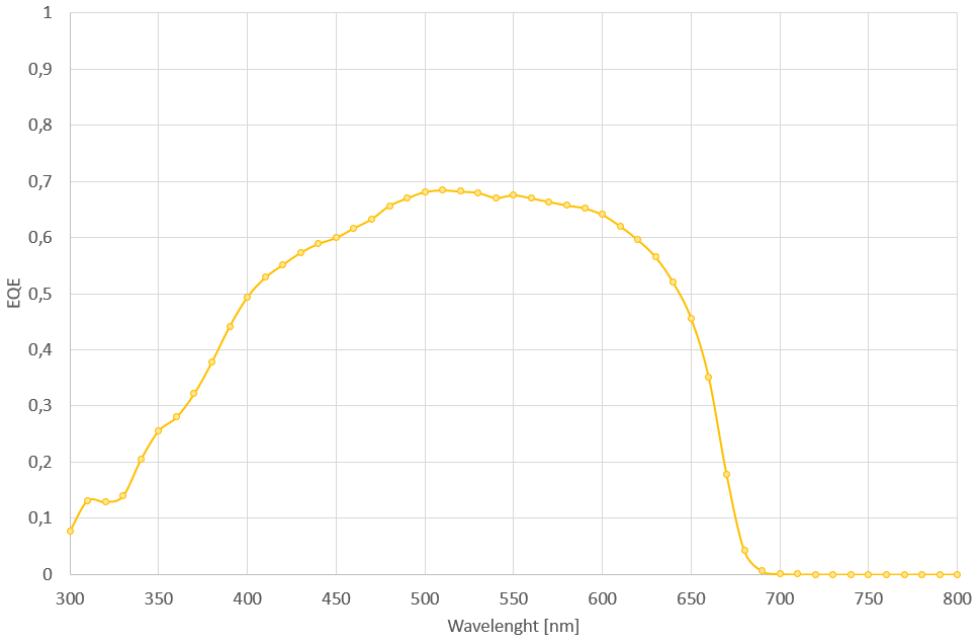

Figure 4.4 QUANTUM EFFICIENCY MEASUREMENT FOR A GaInP CELL (Eg = 663.017 nm).

Looking at figure 4.4 we can see that the external quantum efficiency increases continuously from 300 nm until a maximum value is reached at 510 nm, then decreases slowly until 600 nm and afterwards decreases rapidly until quantum efficiency is zero at 700 nm. The mentioned maximum EQE value achieved for this solar cell is 68.47% at a wavelength of 510 nm.

This behaviour is in well agreement with the value of the band-gap of the GaInP, which is 1.87 eV, that applying formula 3.2 is converted into 663.017 nm, because as we can see in figure 4.4, when this number is approached, the quantum efficiency is reduced as the photons of light that reach the cell are with energies close to the band-gap, and subsequently when the band-gap energy is not reached, there is zero efficiency as the energy of the photons is lesser than that of the material and they will not be absorbed by the GaInP cell.

Analysing this graph, it can be said that this device works in the wavelength range between 300 and 700 nm. Obtaining efficiencies above 60% in the range within 450 and 620 nm. After the wavelength equals 700 nm, there is no external quantum efficiency, since all photons of light with energies below the band-gap of the material, longer wavelengths, will not be absorbed by the cell.

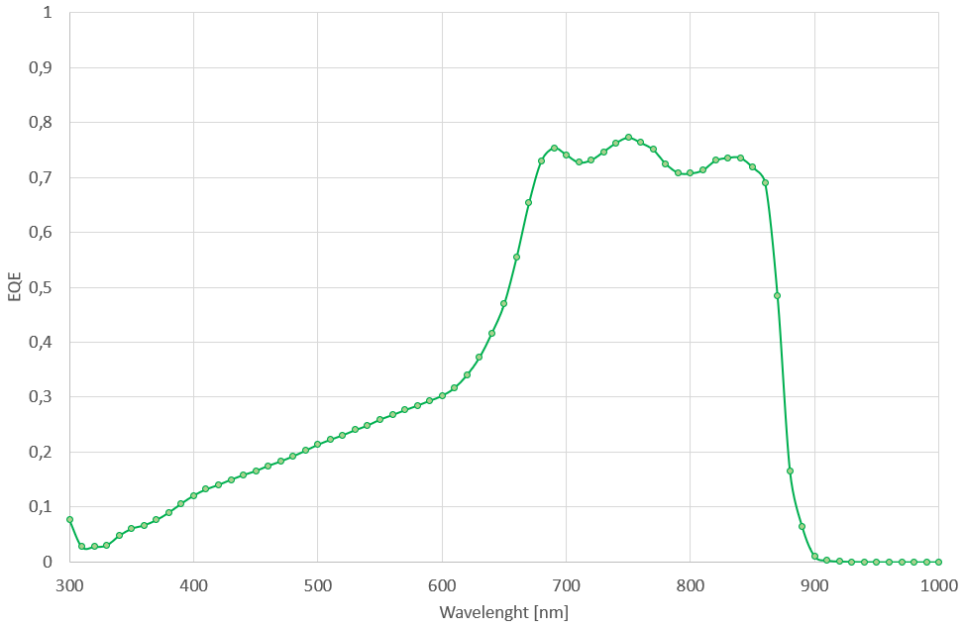

Figure 4.5 QUANTUM EFFICIENCY MEASUREMENT FOR A GaAs CELL (Eg = 873.128 nm).

As we can see in figure 4.5, in this case the path that the external quantum efficiency follows starts with a continuously increase from 310 until 610 nm when it starts to be increased rapidly until 690 nm, at this point, there is a period until 860 nm in which increases and decreases slightly with values around 73%. In this range the maximum value is attained (77.29% at a wavelength of 750 nm). Then it decreases drastically until 930 nm, a point from which there is no longer data from EQE.

The quantum efficiency curve that we obtained in figure 4.5 is consistent with the band-gap of the GaAs, which is 1.42 eV that applying formula 3.2 is converted into 873.128 nm, because as shown in the above graph, when the arriving photons have lower energies than the one of the GaAs band-gap (around 900 nm), the EQE values drop to zero as no photons are absorbed by the cell. As it is going to be shown later in the simulations of section 4.2, EQE losses at low wavelengths are mainly due to recombination effects, while those of high wavelengths are due to the number of photons that reach the absorber layer.

This analysed gallium arsenide device works in the wavelength range between 300 and 930 nm. However, this tested PV cell still has potential to increase its efficiency in the short wavelength region, as it has smaller values of EQE. This improvement can be achieved by reducing the reflection and recombination of the window layer, the front surface (as it will be shown in the simulations presented later in this chapter).

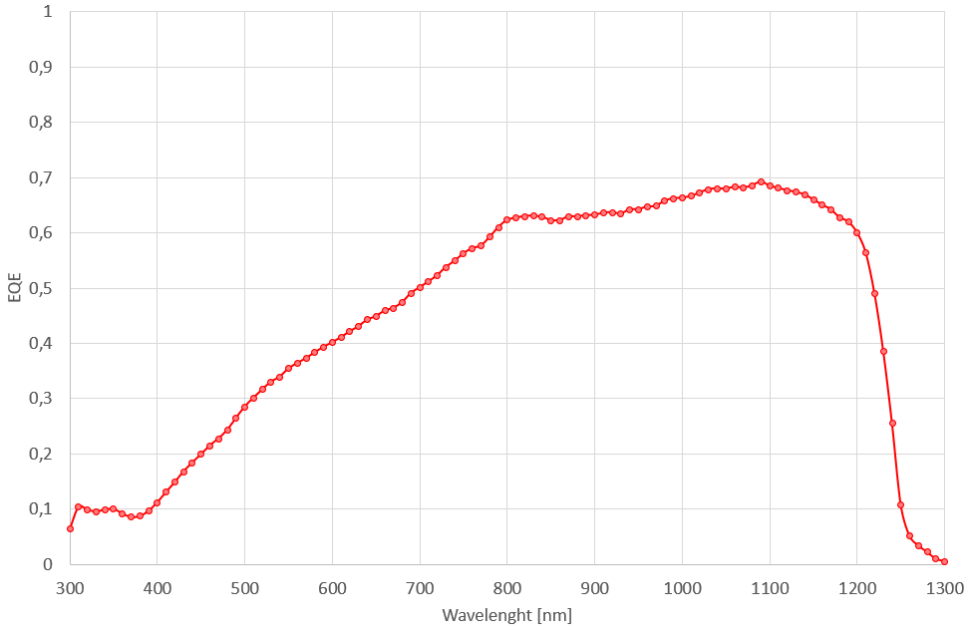

Figure 4.6 QUANTUM EFFICIENCY MEASUREMENT FOR A GaInAs CELL (25% indium and Eg = 1239.841 nm).

It can be seen in figure 4.6 that the external quantum efficiency in this case increases little by little until 800 nm, then there is a range in which it remains relatively in the same point, increasing just from 62.2% to 69.22%, that is the maximum point that the GaInAs cell reaches. Afterwards, it decreases slowly until 1200 nm, and then there is a 50% drop from that point until 1250 nm. Subsequently, there is a period until 1300 nm where the EQE values are really small, it can be just a noise signal.

In the case of GaInAs the band-gap is approximately 1 eV that is transformed into 1239.841 nm by using formula 3.2. The behaviour of the GaInAs is in good agreement with that value because as we can see in figure 4.6 the EQE starts to be reduced around 1200 nm and turns to zero around 1300 nm, the moment at which the band-gap energy is reached.

This GaInAs studied cell, as is the one with the lowest band-gap between the three devices under test, is the one that manages to absorb arriving photons with minor energies. It is taking a wide range of wavelengths, from 300 until 1300 nm, but achieves its best efficiencies between 800 and 1200 nm.

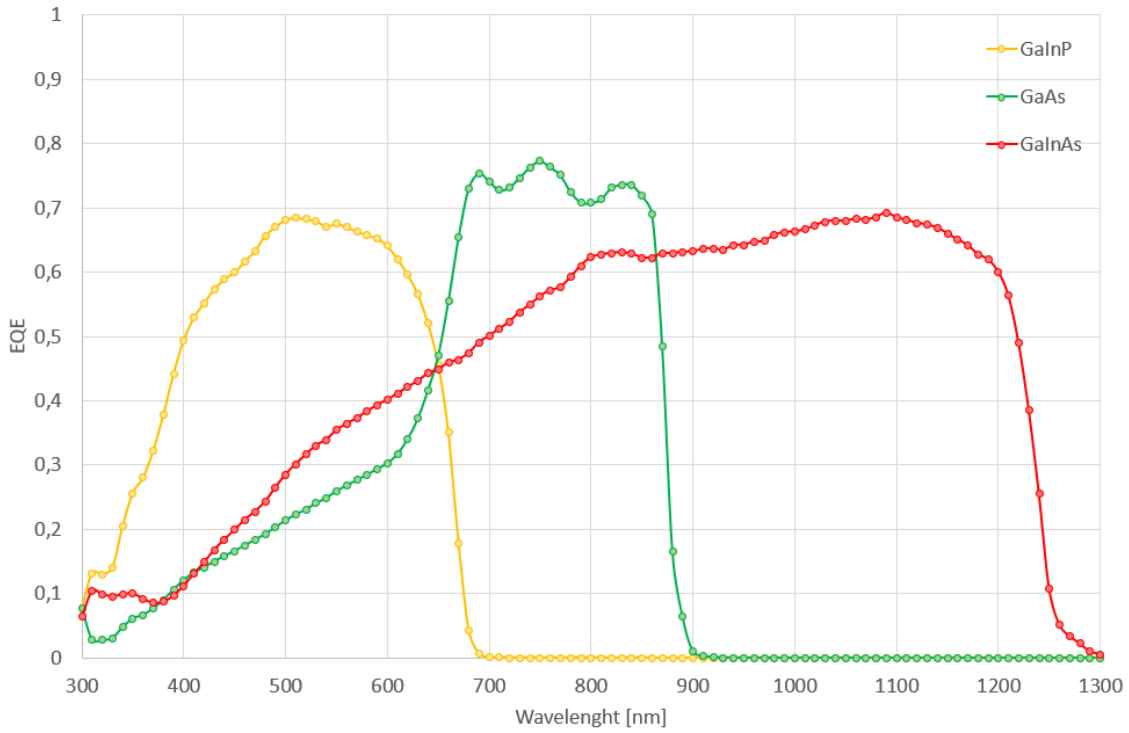

Figure 4.7 EXTERNAL QUANTUM EFFICIENCY OF THE THREE ANALYSED CELLS.

Figure 4.7 is the combination of the previous three graphs. Although all of them are single-junction cells made by III-V materials, each of them captures different ranges of wavelength since they are made of different semiconductors. As explained in chapter 2, the addition of several layers of different materials in the same solar cell can suppose a huge increase in its quantum efficiency, since there is a bigger field of wavelengths covered. Therefore, more photons could enter the cell.

In this particular case, if a cell were formed with these analysed sub-cells, the order of placement would be the GaInP at the top, as it has the ability to absorb particles with higher energies, then in the middle the GaAs cell and at the bottom the GaInAs, that in this case, as it was explained in section 3.1.3 is composed of approximately 25% of indium, achieving by this way a cell with a band-gap of 1 eV.

In the three cases at the end of the curve the EQE values are lower because the energy of the arriving photons is close to the energy band-gap, afterwards it continues decreasing until the light arrives with an energy lower than that of the band-gap and therefore the photons will not be absorbed by the cells.

Once the external quantum efficiency data for the three tested solar devices have been obtained, the photocurrent that each cell produces is calculated using a program developed by Iván García Vara (IES 2005). In this program, the efficiency data of each of the cells is introduced, the application calculates the integral of the quantum efficiency introduced taking the contribution of all the wavelengths, following equation 2.20, and the value of the photocurrent is acquired.

Table 4.1 PHOTOCURRENT OBTAINED PER EACH CELL.

Devices under test	**I_L (mA/cm^2)**
GaInP	9.631
GaAs	14.908
GaInAs	24.914

Evaluating the photocurrent results obtained for the different cells, exposed in table 4.1, it is seen that there is a significant variation between them. What causes it is the influence of the wavelengths. In the case of GaInAs, the highest photocurrent value is achieved as it is the device with the lower band-gap, 1 eV, which implies a greater range of wavelengths (300 to 1300 nm), so the incorporation of photons coming with minor energies increases the current generation.

If the three cells were put together forming a III-V multi-junction solar cell, the resulting photocurrent will be drastically increased.

4.2 Analysis of the material's properties effect on the quantum efficiency

As previously explained in section 2.3.1, a single junction cell of III-V materials is made up of three regions: window, emitter and base. Each of these regions has its own parameters that can be modified since they are modulable. Subsequently, the explanation of how some of these parameters affect the quantum efficiency of the cell is going to be developed with the aim of understanding its effects so that we will be able to offer an optimal structure to reproduce experimentally.

In order to see how these modifications affect the quantum efficiency we have worked with Python, using a code written in the Physics Department of the UC3M. The cell under study is a single-junction GaAs cell with a window of GaInP, a n-type emitter and a p-type base.

The following parameters have been considered as the reference starting point for the simulations. These parameters correspond to a standard-quality GaAs solar cell.

Table 4.2 REFERENCE PARAMETERS.

Layers	Diffusion length (μm)	Surface recombination velocity (cm/s)	Thickness (μm)	Minority carrier lifetime (ns)	Doping (particles cm^3)
Window	0.7	5e6	0.05	0.9	-
Emitter	0.2	100.0	0.15	0.4	8e17
Base	10.0	100.0	3.5	27.0	3e17

In this investigation, it has been studied the internal quantum efficiency (IQE), as it does not take into account any losses, as explained in section 2.3.3 so the contribution of each parameter can be analysed more straightforwardly.

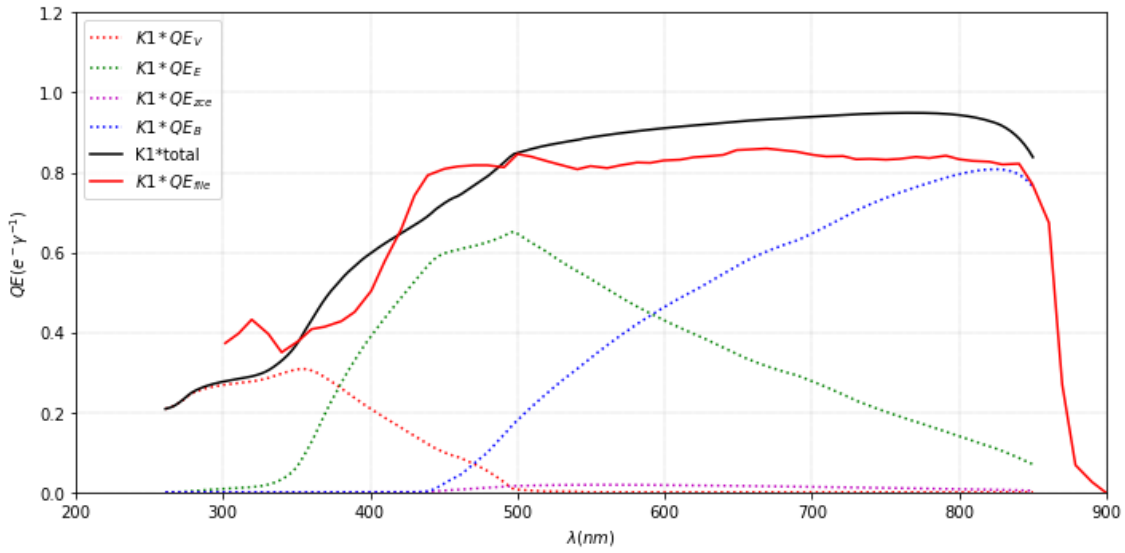

Figure 4.8 SIMULATED IQE WITH REFERENCE PARAMETERS.

Figure 4.8 shows the internal quantum efficiency obtained when introducing in the Python code the standard parameters above mentioned. The black line corresponds to the total IQE, i.e. the most interesting one in this analysis, the red line is the experimental curve obtained for a standard GaAs and the blue, green and red dotted lines are the contribution of each separate region (i.e. base, emitter and window, respectively) to the IQE. On this basis, the improvement of the efficiency of this cell will be studied by modifying its modular parameters.

- **Window parameters**

Surface recombination velocity:

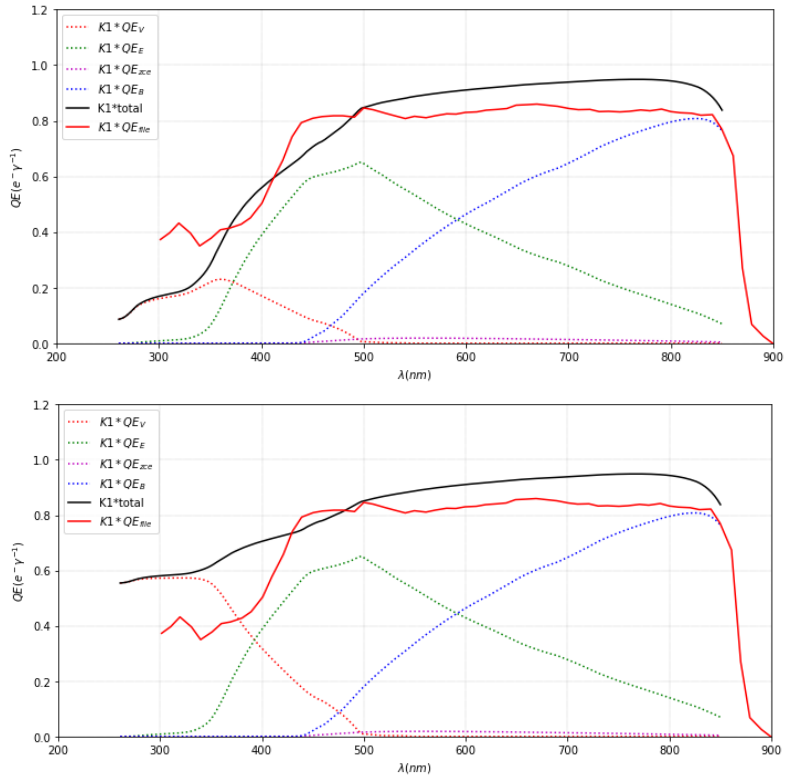

Figure 4.9 SIMULATED IQE WITH SURFACE RECOMBINATION VELOCITY 1. INCREASED (S_V = 100e10 #cm/s) AND 2. DECREASED (S_V = 5e5 #cm/s).

Recombination effects reduce quantum efficiency, and in the window layer it is really easy for recombination to occur as there are multiple blemishes and impurities at the surface. Looking at figure 4.8 we can see that this cell has the potential to increase its efficiency in the short wavelength region between 300 and 500 nm. For that reason, the surface recombination velocity of the window layer is studied.

With the simulations performed, represented in figure 4.9, we can see that the short wavelength range is altered with the changes in the recombination velocity. In the first graph it is shown that the increase of this parameter decreases the efficiency considerably. A high recombination affects the blue part of the solar spectrum (figure 2.20). On the contrary, there is a huge positive change when reducing the recombination velocity on the window layer. The efficiency is increased from a 20% in the basis case, until almost a 60% and continues increasing until 500 nm when we recover the original shape of the curve.

Thickness:

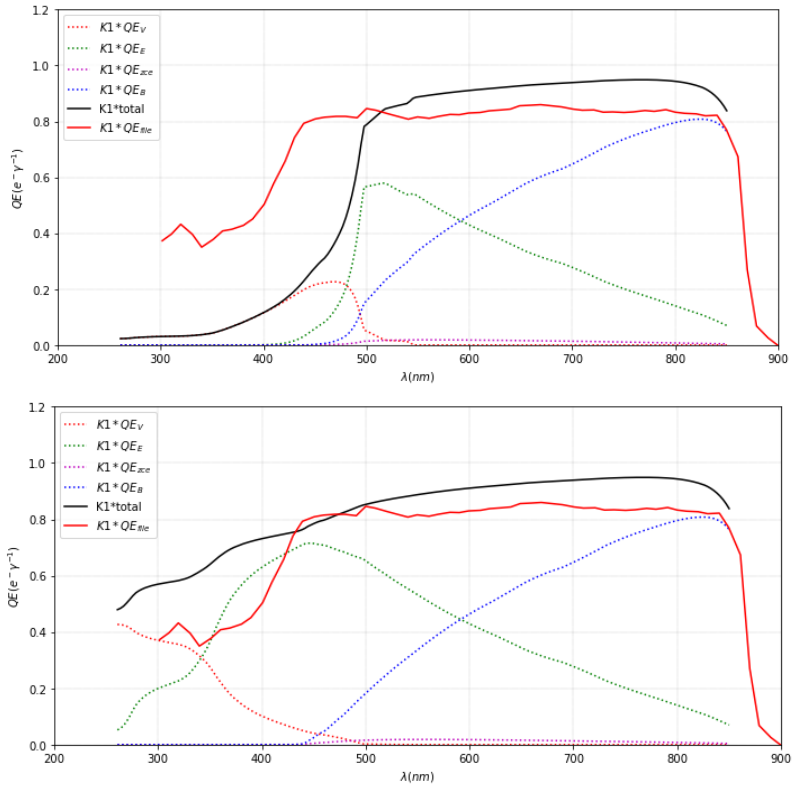

Figure 4.10 SIMULATED IQE WITH THICKNESS 1. INCREASED (W_V=0.05 #um) AND 2. DECREASED (W_V=0.015 #um).

The thickness of the window layer is a very important parameter in improving the efficiency of the tested GaAs cell. In the first graph of figure 4.10 we can see that with the increase of the thickness the efficiency is drastically reduced. The cause of this drop is that with the increase of the thickness there are more photons absorbed but not all of them arrive at the absorber layer, which is necessary to participate in the energy conversion process. Therefore, as shown in the second graph of figure 4.10, it is a better option to reduce the thickness of the window layer to increase the efficiency, but without reducing it to zero, because if so, the window layer will disappear and with it its contribution would therefore be null.

- **Emitter parameters**

Diffusion length and minority carrier lifetime:

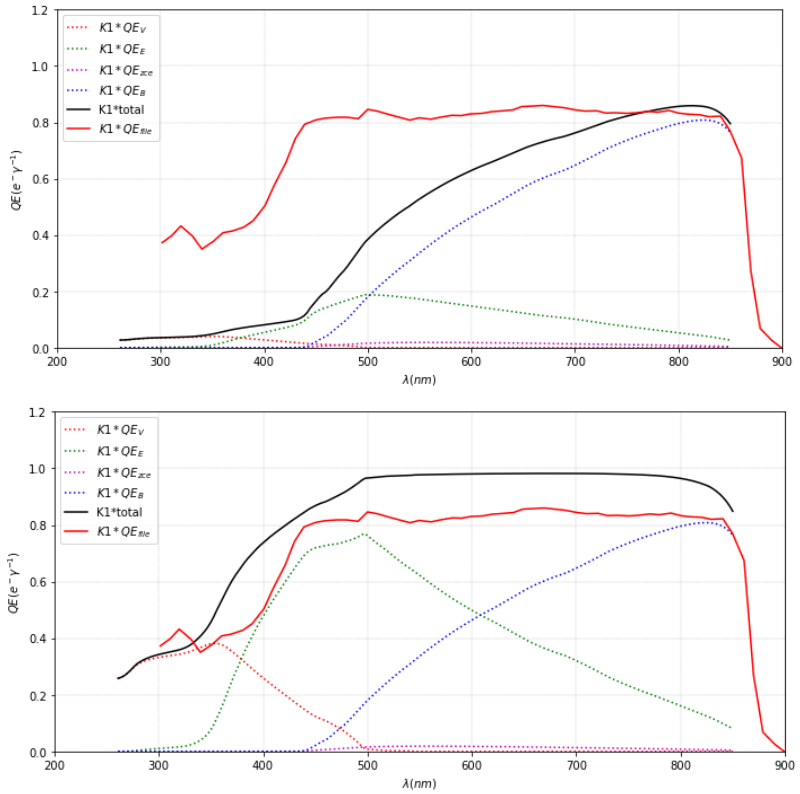

Figure 4.11 SIMULATED IQE WITH DIFFUSION LENGTH AND MINORITY CARRIER LIFETIME 1. DECREASED (L_E=0.05 #um, tau_E=0.1 #ns) AND 2. INCREASED (L_E=0.5 #um, tau_E=0.7 #ns).

In figure 4.11 we have the representation of the modifications in diffusion length and minority carrier lifetime. These two parameters are linked, so they were varied together. If the diffusion length is high, it means that the minority carriers can travel a long distance without recombining, so their lifetime is high as well, and vice versa.

On these above graphs (figure 4.11) is depicted that if the diffusion length is low, the quantum efficiency is also low in the lower and middle wavelength's region, which corresponds to the photons that must be absorbed in the emitter region. This is happening because the collection probability is affected by these factors and there are less photons being absorbed. On the other hand, in the second graph it is shown that with the increase of these both parameters the efficiency is improved. However, experimentally these parameters are difficult to tune. Contrary to what happens with the doping level or the thickness, (i.e. parameters that can be easily modulated experimentally), the minority carrier lifetime depends on the quality of the grown material. Therefore, even if the highest value is always pursued, it is difficult to attain.

Thickness:

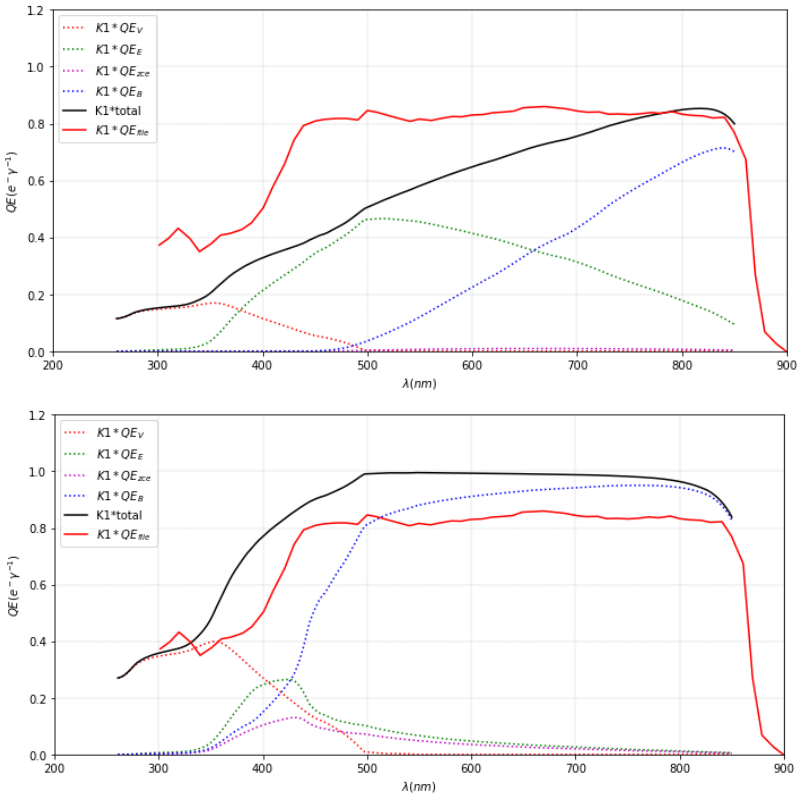

Figure 4.12 SIMULATED IQE WITH THICKNESS 1. INCREASED (W_E=0.3 #um) AND 2. DECREASED (W_E=0.01 #um).

Having a thicker emitter layer reduces the efficiency in almost all the wavelength range. The reason for this fall is that the absorption of the light is not ideal; there are electron-hole pairs generated in the layer close to the front contact of the solar cell, which can provoke losses in electrons and then less pairs in the GaAs layer.

Analysing both representations in figure 4.12 we can see that a thinner layer will be useful to the efficiency of the cell. Although always keeping in mind that the thickness must be within a range because if there is a wide reduction, the emitter layer would disappear and with it the solar cell as without an emitter there is no solar cell.

- **Base parameters**

Diffusion length and minority carrier lifetime:

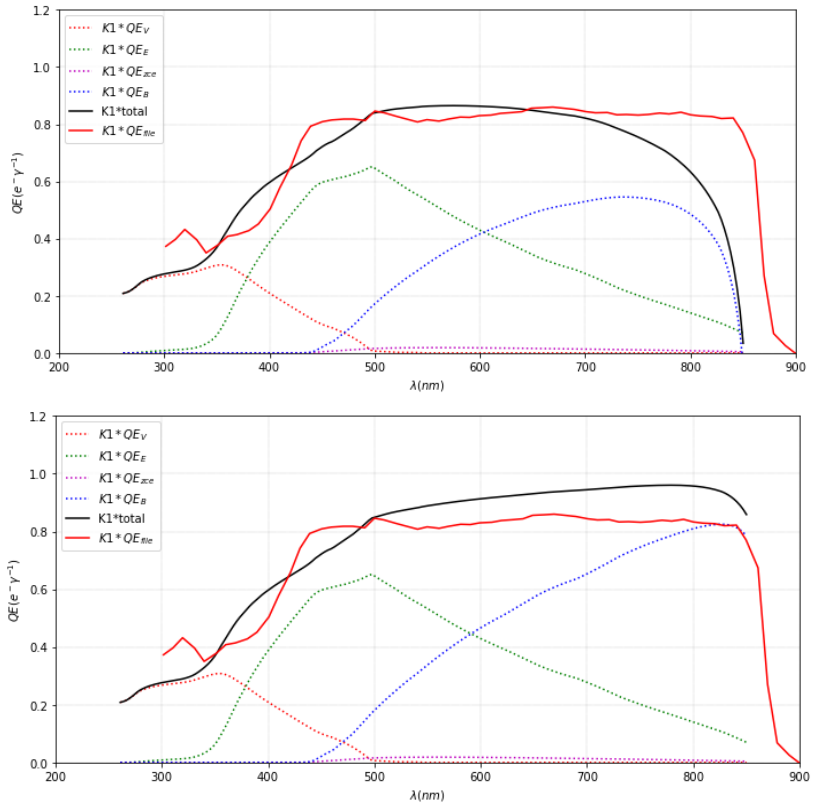

Figure 4.13 SIMULATED IQE WITH DIFFUSION LENGTH AND MINORITY CARRIER LIFETIME 1. DECREASED (L_B=2.85 #um, tau_B=7.71 #ns) AND 2. INCREASED (L_B=20 #um, tau_B=37 #ns).

Figure 4.13 represents the effect of the variation of the minority carrier lifetime parameters of the base region in the IQE. When the diffusion length and the minority carrier lifetime is low, the quantum efficiency at higher wavelengths (which corresponds to the base region) descends quickly until it reaches practically 0%, there are almost non photons absorbed.

Conversely, with the augmentation of both parameters there is a slight increase in quantum efficiency.

Thickness:

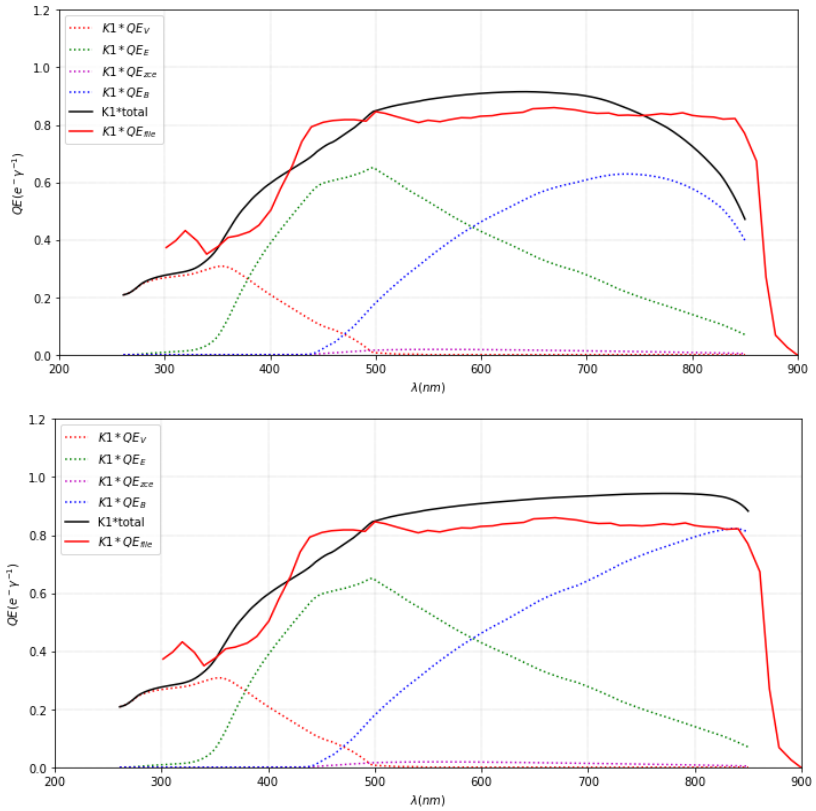

Figure 4.14 SIMULATED IQE WITH THICKNESS 1. DECREASED (W_B=1 #um) AND 2. INCREASED (W_B=5 #um).

In figure 4.14 we can see a different case than in the emitter layer thickness. The base layer finds improvements with increasing its thickness. Based on the fact that from the beginning, the thickness of the base layer is much greater than that of the emitter.

If the thickness is reduced, at higher wavelengths, the efficiency decreases.

After the study carried out for the different parameters and layers of the GaAs cell analysed, combining all the discovered features to obtain greater efficiency in each layer, it is obtained the following representation of the IQE introducing the following parameters modified from the initial basis.

Table 4.3 MODIFIED PARAMETERS.

Layers	**Diffusion length (µm)**	**Surface recombination velocity (cm/s)**	**Thickness (µm)**	**Minority carrier lifetime (ns)**	**Doping (particles cm^3)**
Window	0.7	2e6	0.025	0.9	-
Emitter	0.35	100.0	0.09	0.55	8e17
Base	14.0	100.0	4.05	31.0	3e17

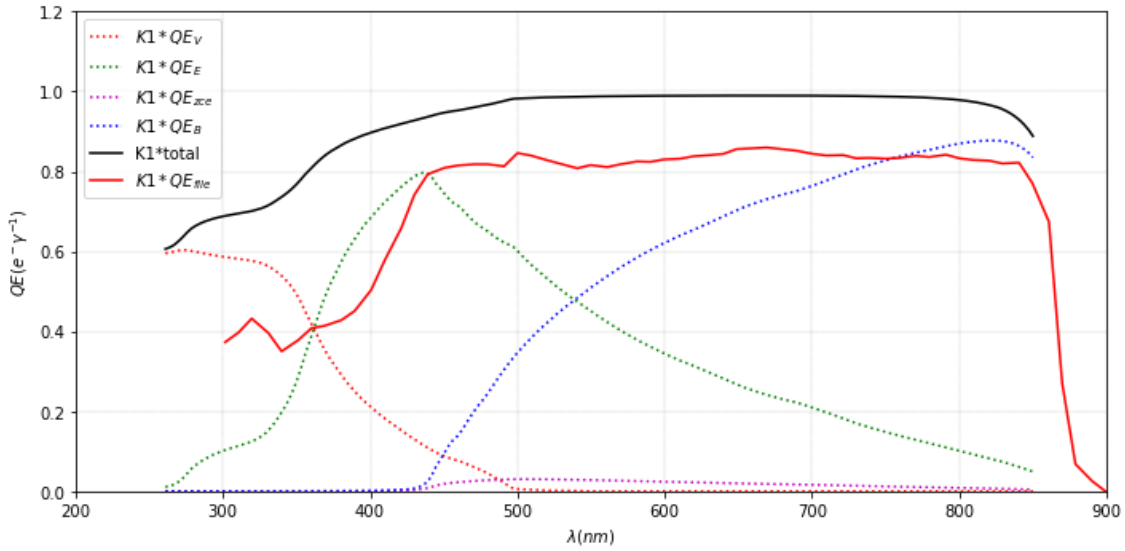

Figure 4.15 SIMULATED IQE WITH MODIFIED PARAMETERS.

It can be seen that with all the previous mentioned changes included in this figure 4.15, using the same GaAs solar cell with modifications, it is obtained an IQE with highly improved values.

The region of lower wavelengths, when the starting parameters were introduced (figure 4.8) was around 20% at 300 nm and it increased continuously but slowly until 80% was reached at 500 nm. On the other hand, with the new theoretical upgrades (figure 4.15), it is starting around 60% and at higher wavelengths it is almost attaining 100% quantum efficiency, achieving the maximum IQE value around 500 nm, because of the sum of the contributions of the base and the emitter. In general, the internal quantum efficiency remains close to 100%, indicating excellent lifetimes and diffusion length of the minority carriers.

The thickness of the active layers, emitter and base, ($W_E + W_B$) must be around 4 and 4.5 µm to absorb the 95% of the incident photons [49]. The thickness of the emitter layer must remain small, as demonstrated in the simulations in figure 4.12, to compensate for its restrained diffusion length and lifetime of its carriers. In our studied theoretical case, we are working with a thickness of the active layers equal to 4.14 µm.

By applying these described changes to a new solar cell with the same material composition (GaAs), we could enhance the capture and absorption of photons coming from the sun in the different layers, which leads to a notable rise in quantum efficiency, which was the main reason for the development of these simulations.

With the description and analysis of the previous simulations, the effect of the most important modular parameters of each layer (window, emitter and base) on the photovoltaic behaviour of a GaAs solar cell have been studied and understood.

This has been a theoretical investigation. Therefore, it must be taken into account that not all parameters are easy to modulate experimentally, such as the minority carrier lifetime. For that reason, this developed review must be simply used as a guide of how to theoretically optimize the quantum efficiency of a solar cell. Moreover, the study aims to be a feedback tool for the experimental cell growth processes, allowing greater efficiencies to be obtained.

CHAPTER 5

CONCLUSIONS, FUTURE WORKS, AND COST ANALYSIS

5. CONCLUSIONS, FUTURE WORKS, AND COST ANALYSIS

The characterization of solar cells is known to be a key factor as a feedback tool for improving the efficiencies of the solar devices. In this respect, this project was aimed at proposing a technique (i.e. spectral response) which can properly characterize these devices, as well as to understand how the different parameters of the solar cell (i.e. band-gap, doping levels, thickness, material quality) affect the electrical response of the device. To accomplish this objective, it has been studied the working principle of the technique with the final aim of installing a Spectral Response equipment in the Physics Department of the UC3M for a research line on third generation solar cells.

After setting-up the equipment, it has been calibrated by means of measuring a reference device (i.e. silicon solar cell), whose spectral response under standard measurement conditions was known.

Once the calibration was carried out, three different III-V cells, with different band-gaps were aimed to be measured. However, due to some problems, and limitations, it was not possible to obtain the proper results. First of all, it has to be mentioned that the equipment is in early stages of operation, there are things that need to be improved specially the way to measure with the test probes, that is a somewhat "primitive" way. Moreover, it would be necessary to better calibrate the light spot since as it was depicted in figure 3.6, the III-V solar cells have a very small size (around 5 mm), and the spot must be more precise. We are measuring the correction coefficient, which is defined by the unit of active area, for that reason it is compulsory that the spot impact inside of the cell in all the cases, otherwise, if it only illuminates part of the cell, the measurements will not be correct.

After numerous attempts to overcome the limitations, an improvement was achieved in the obtained results but without reaching the due ones. This circumstance led us to use in our study data from the measurements carried out at the IES-UPM. The analysis and interpretation of these data leads us to the following conclusions:

With the analysis of the results obtained with the characterization of the cells, presented in the first part of chapter 4, we have been able to verify the relationship between the material's band-gap and the quantum efficiency. The greater the energy of the band-gap, the smaller the efficiencies reached and the range of wavelengths. As the band-gap energy decreases, the efficiency increases as does the absorption of light wavelengths available. Consequently, materials to form multi-junction solar cells are wisely selected to absorb as much solar spectrum as possible.

This previous analysis leads us to prove that the spectral response technique is good for the photoelectric characterization of solar cells.

We have also described a different approach for a potential increase of the efficiency of multi-junction solar cells based on III-V materials. By means of a simulation tool, we are able to understand the effect of different modular parameters on the quantum efficiency of the device, serving as a feedback tool for future experimental studies.

In this respect, we have theoretically studied the effect of parameters such as: surface recombination velocity, thickness, diffusion length and minority carrier lifetime on the performance of a standard GaAs solar cell. The simulations were performed using a Python code developed by the UC3M Physics Department.

On one hand, we have the thickness of the window and emitter layers that the thinner it is, the better yields we are going to get at lower wavelengths, but on the contrary, the wider the base, the more efficient the cell is.

In the case of the material quality (i.e. diffusion length and minority carrier lifetime) they are working in the same way for both layers (emitter and base). They have to be increased so that the minority carriers can travel long distances without recombining. Related to this phenomenon, the surface recombination velocity must be reduced in the window layer as recombination effects reduce quantum efficiency at short wavelengths.

The cost analysis of this project includes the material and equipment expenses and also the cost of the needed staff in the laboratory to continue the line of research of this project for the characterization of different solar devices to improve the manufacturing process and improve the efficiencies of future cells.

Table 5.1 ESTIMATED COSTS REALTED TO THE INVESTIGATION.

Material/personnel		**Cost**
Reference cell		-
III-V solar cells		-
EQE characterization equipment	Light source	17,975 €
	Chopper	1,447 €
	Pre-amplifier	3,142 €
	Lock-in	2,099 €
	Test probes (2)	1,390 €
Python license		0 €
Engineer		37,900 €/year

There would not be any direct expense of the cells studied but there would be an indirect one for the cells being brought to us since we do not buy them, but they lend the devices to us to study them (collaborations with different Universities and Research Centres).

There is a potential way under development for the improvement in efficiency of third generation solar cells, especially in III-V multi-junction solar cells that were the technologies studied during this bachelor thesis. Nevertheless, there is still a wide range of research needed to move from laboratory scale demonstrations to potential commercial production of these multi-junction solar cells but gently, there are more possibilities of creating more efficient and lower cost solar cells that can be competitive with the traditional silicon-based cells.

CHAPTER 6
REFERENCES

6. REFERENCES

[1] IRENA, Transformación energética mundial: hoja de ruta hasta 2050. Abhu Dhabi: International Renewable Energy Agency, 2018. [Online]. Available at: https://irena.org/-/media/Files/IRENA/Agency/Publication/2018/Apr/IRENA_Global_Energy_Transformation_2018_summary_ES.pdf?la=en&hash=A5492C2AAC7D8E7A7CBF71A460649A8DEDB48A82

[2] IEA, "Global energy demand to plunge this year as a result of the biggest shock since the Second World War". International Energy Agency. https://www.iea.org/news/global-energy-demand-to-plunge-this-year-as-a-result-of-the-biggest-shock-since-the-second-world-war (Accessed: 26th July 2021).

[3] IEA, Global Energy Review 2020 The impacts of the Covid-19 crisis on global energy demand and CO2 emissions. France: International Energy Agency, 2020. [Online] Available at: https://iea.blob.core.windows.net/assets/7e802f6a-0b30-4714-abb1-46f21a7a9530/Global_Energy_Review_2020.pdf

[4] Us Energy Information Administration, "Energy-related CO2 emissions", in International Energy Outlook 2016. United States: CreateSpace Independent Publishing Platform, 2016, 139-148.

[5] European Parliament, European policies on climate and energy towards 2020, 2030 and 2050. 2019. [Online] Available at: https://www.europarl.europa.eu/RegData/etudes/BRIE/2019/631047/IPOL_BRI(2019)631047_EN.pdf

[6] United Nations. "El Acuerdo de París". United Nations Framework Convention on Climate Change. https://unfccc.int/es/process-and-meetings/the-paris-agreement/el-acuerdo-de-paris. (Accessed: 28th July 2021).

[7] European Commission. "2050 long-term strategy". European Commission website. https://ec.europa.eu/clima/policies/strategies/2050_en. (Accessed: 28th July 2021).

[8] European Commission. "2020 climate & energy package". European Commission website. https://ec.europa.eu/clima/policies/strategies/2020_en. (Accessed: 27th July 2021).

[9] Comisión Europea. "Marco sobre clima y energía para 2030". European Commission website. https://ec.europa.eu/clima/policies/strategies/2030_es#:~:text=Objetivos%20clave%20para%202030%3A,mejora%20de%20la%20eficiencia%20energ%C3%A9tica. (Accessed: 27th July 2021).

[10] P. D'Aprile, H. Engel, G. van Gendt, S. Helmcke, S. Hieronimus, T. Nauclér, D. Pinner, D. Walter, M. Witteveen, Net-Zero Europe Decarbonization pathways and socioeconomic implications. McKinsey & Company, 2020. [Online]. Available at: https://www.mckinsey.com/business-functions/sustainability/our-insights/how-the-european-union-could-achieve-net-zero-emissions-at-net-zero-cost#

[11] J. L. Balenzategui Manzanares, Fundamentos de la conversión fotovoltaica: la célula solar. EOI, 2007. [Online]. Available at: https://www.eoi.es/es/savia/publicaciones/20215/fundamentos-de-la-conversion-fotovoltaica-la-celula-solar

[12] NREL, Best Research-Cell Efficiency Chart. National Renewable Energy Laboratory, 2021. [Online] Available at: https://www.nrel.gov/pv/cell-efficiency.html

[13] IEA, Snapshot of Global PV Markets 2021. Technology Collaboration Programme by IEA, 2021. [Online] Available at: https://iea-pvps.org/snapshot-reports/snapshot-2021/

[14] IEA, "Renewables 2020, Solar PV". International Energy Agency. https://www.iea.org/reports/renewables-2020/solar-pv. (Accessed: 28th July 2021).

[15] T. Zhang, M. Wang, H. Yang, A Review of the Energy Performance and Life-Cycle Assessment of Building-Integrated Photovoltaic (BIPV) Systems. Hong Kong: MDPI, 2018. [Online]. Available at: https://www.researchgate.net/publication/328948832_A_Review_of_the_Energy_Performance_and_Life-Cycle_Assessment_of_Building-Integrated_Photovoltaic_BIPV_Systems

[16] Y. Kuang, J.K. Rath, M. Di Vece, L. van Dijk, Elongated nanostructures for radial junction solar cells. IOP Publishing, 2013. [Online]. Available at: https://www.researchgate.net/publication/257309627_Elongated_nanostructures_for_radial_junction_solar_cells

[17] S. Sadewasser, M. CH. Lux-Steiner, S. Lehmann, Tetrahedral chalcopyrite quantum dots for solar-cell applications. American Institute of Physics, 2011. [Online]. Available at: https://www.researchgate.net/publication/234892466_Tetrahedral_chalcopyrite_quantum_dots_for_solar-cell_applications

[18] G. Conibeer, Third-generation photovoltaics. Society of Photo-optical Instrumentation Engineers, 2007. [Online] Available at: https://www.researchgate.net/publication/228885845_Third-generation_photovoltaics

[19] NREL, Best Research-Cell Efficiencies: Emerging Photovoltaics. National Renewable Energy Laboratory, 2021. [Online] Available at: https://www.nrel.gov/pv/assets/pdfs/cell-pv-eff-emergingpv.202001042.pdf

[20] K. Sharma, V. Sharma, S.S. Sharma, "Dye-Sensitized Solar Cells: Fundamentals and Current Status". Springer Open. https://nanoscalereslett.springeropen.com/articles/10.1186/s11671-018-2760-6. (Accessed: 30th July 2021).

[21] M.A. Mingsukang, M.H. Buraidah, A.K. Arof, "Third-Generation-Sensitized Solar Cells", in Nanostructured Solar Cells. Narottan Das, 2017, 7-31.

[22] D. Martín Martín, 6 November 2020, "DISEÑO, FABRICACIÓN Y CARACTERIZACIÓN DE CÉLULAS SOLARES MULTIUNIÓN PEROVSKITA/SILICIO CON EFICIENCIAS SUPERIORES AL 30%". BOE número 293, Sec. II.B., páginas 96936 a 96960.

[23] Solar Energy Technologies Office, "Organic Photovoltaics Research". Office of Energy & Renewable Energy. https://www.energy.gov/eere/solar/organic-photovoltaics-research. (Accessed: 30th July 2021).

[24] B. Afework, J. Hanania, K. Stenhouse, B. Yyelland, J. Donev, "Photovoltaic cell". University of Calgary. https://energyeducation.ca/encyclopedia/Photovoltaic_cell (Accessed: 21st June 2021).

[25] Planet Energies. "How Does a Photovoltaic Cell Work?". April 2019. [Online] Available at: https://www.planete-energies.com/en/medias/close/how-does-photovoltaic-cell-work (Accessed: 21st June 2021)

[26] N. L. Nguyen, N. Colonna, A. Ferretti, N. Marzari, Koopmans-compliant spectral functionals for extended systems. American Physical Society, 2017. [Online]. Available at: https://www.researchgate.net/publication/319349795_Koopmans-Compliant_Spectral_Functionals_for_Extended_Systems

[27] A. K. Sood, J. W. Zeller, Y. R. Puri, C. Rouse, P. Haldar, H. Efstathiadis, N. K. Dhar, P. S. Wijewarnasuriya, "SiGe Focal Plane Array Detector Technology for Near-Infrared Imaging". International Journal of Engineering Research and Technology, vol. 10, nº 1, pp. 81-103, 2017. [Online]. Available at: https://www.researchgate.net/publication/318111138_SiGe_Focal_Plane_Array_Detector_Technology_for_Near-Infrared_Imaging

[28] A. Geižutis. (2019). Repetition of 1st semester (2nd part of 2). [PowerPoint presentation].

[29] W. Shockley, Electrones and Holes in Semiconductors with applications to transitor electronics. 7th ed. Princeton, New Jersey: D. van Nostrand Company, Inc, 1951.

[30] C. M. Hussain, "Engineeered Nanomaterials for Energy Applications", in Handbook of Nanomaterials for Industrial Applications. United States: Elseiver, 2018, 721-767.

[31] M. Iqbal, An Introduction to Solar Radiation. Vancouver, British Columbia: Academic Press, Inc, 1983.

[32] J. A. Duffie, W. A. Beckman, Solar Engineering of Thermal Processes. 4th ed. Ney Jersey: John Wiley & Sons, Inc, 2013.

[33] R. E. Rojas Hernández, "Caracterización espectral de células solares comerciales", Trabajo fin de máster, Dpto. de Física, Universidad de Salamanca, Salamanca, España, 2011. [Online]. Available at: https://lbt.usal.es/wp-content/uploads/2015/12/TFM.pdf

[34] R. J. Moreno Sáez, "Modelado del espectro solar y su influencia en el funcionamiento de módulos fotovoltaicos de lámina delgada", Tesis doctoral, Dpto. de Lenguajes y Ciencias de la Computación, Universidad de Málaga, Málaga, España, 2014. [Online]. Available at: https://riuma.uma.es/xmlui/handle/10630/7689

[35] J. H. Walker, R. D. Saunders, J. K. Jackson, D. A. McSparron, NBS MEASUREMENT SERVICES: SPECTRAL IRRADIANCE CALIBRATIONS. U.S. Washington: Department of commerce, National Bureau of standards, 1987. [Online]. Available at: https://books.google.es/books?hl=es&lr=&id=PTD9tUCF8G4C&oi=fnd&pg=PA1&dq=spectral+irradiance+definition&ots=ljMeQefDpc&sig=XT6U_TXzIBwgb5oN1JMMCfWRN9I#v=onepage&q&f=false

[36] R. Garner. "Solar Irradiance". National Aeronautics and Space Administration. https://www.nasa.gov/mission_pages/sdo/science/solar-irradiance.html (Accessed: 16th July 2021).

[37] B. Galiana Blanco (2015). Characterization of solar cells. [PowerPoint presentation].

[38] B. K. Ghosh, C. NJ. Weoi, A. Islam, S. K. Ghosh, Recent progress in Si hetero-junction solar cell: A comprehensive reviews. Malaysia: 2017. [Online]. Available at: http://dx.doi.org/10.1016/j.rser.2017.07.022

[39] E. García-Tabarés Valdivieso, "MOVPE GROWTH OF III-V SEMICONDUCTORS ON SILICON FOR THIRD GENERATION SOLAR CELLS", Tesis doctoral, Dpto. De Electrónica Física, Universidad Politécnica de Madrid, Madrid, España, 2015. [Online]. Available at: http://oa.upm.es/36264/1/ELISA_GARCIA_TABARES_VALDIVIESO_01.pdf

[40] E. Fernández Férnandez, "MODELIZACIÓN Y CARACTERIZACIÓN DE CÉLULAS SOLARES III-V MULTIUNIÓN Y DE MÓDULOS DE CONCENTRACIÓN", Tesis doctoral, Dpto. de Electrónica, Universidad de Santiago de Compostela, Santiago de Compostela, España, 2012. [Online]. Available at: https://dialnet.unirioja.es/servlet/tesis?codigo=109890

[41] "Célula fotovoltaica multiunión". Copro. https://copro.com.ar/Celula_fotovoltaica_multiunion.html. (Accessed: 11th August 2021).

[42] N. Žurauskienė, (2019). Photovoltaic Energy Systems. [PowerPoint presentation].

[43] K. Ananda-Rao, Y.Matar, N. H. Baharudin, A. M. Abdullah, 2019, "Design of MMPT charge controller using zeta converter for battery integrated with solar Photovoltaic (PV) system" Journal of Physics: Conference Series, doi: 10.1088/1742-6596/1432/1/012058.

[44] M.Barukčić, Ž.Hederić, Ž.Špoljarić, "The estimation of I–V curves of PV panel using manufacturers' I–V curves and evolutionary strategy". Energy Conversion and Management, vol. 88, pp. 447-458, 2014. [Online]. Available at: https://www.sciencedirect.com/science/article/pii/S0196890414007766

[45] McGraw-Hill Dictionary of Scientific & Technical Terms. The McGraw-Hill Companies, Inc. 2003.

[46] J. Meydbray, K. Emery andS. Kurtz, "Pyranometers and Reference Cells, What's the Difference?", PV Magazine, April 2012. [Online]. Available at: https://www.nrel.gov/docs/fy12osti/54498.pdf. (Accessed: 24th July 2021)

[47] P. Martín Díez, (2020). Caracterización de células de referencia para la medida de la Eficiencia Cuántica Externa. [PowerPoint presentation]

[48] M. W. Wanlass, S. P. Ahrenkiel, D. S. Albin, J. J. Carapella, A. Duda, K. Emery, J. F. Geisz, K. Jones, Sarah Kurtz, T. Moriarty, and M. J. Romero, "GaInP/GaAs/GaInAs Monolithic Tandem Cells for High-Performance Solar Concentrators", presented in International Conference on Solar Concentrators for the Generation of Electricity or Hydrogen, Scottsdale, Arizona, 1-5 May, 2005. [Online]. Available at: https://www.nrel.gov/docs/fy05osti/38646.pdf

[49] I. Rey-Stolle Prado, "Desarrollo de Células Solares de GaAs para Concentraciones Luminosas Muy Elevadas", Tesis doctoral, Dpto. de Electrónica Física, Universidad Politécnica de Madrid, Madrid, España, 2001. [Online]. Available at: http://www.upm.es/observatorio/vi/index.jsp?pageac=actividad.jsp&id_actividad=44451

[50] K. Frohna, S. D. Stranks, "7 – Hybrid perovskites for device applications". Handbook of Organic Materials for Electronic and Photonic Devices, Second Edition. Woodhead Publishing Series in Electronic and Optical Materials 2019, 211-256. [Online]. Available at: https://www.sciencedirect.com/science/article/pii/B9780081022849000073

[51] S. Meroli. "The Minority Carrier Lifetime in Silicon Wafer". Stefano Meroli: life of an engineer at CERN. https://meroli.web.cern.ch/Lecture_lifetime.html. (Accessed: 23rd August 2021).

[52] B. Rastegar, "Surface Recombination Velocity and Bulk Lifetime in GaAs and InP", Master Thesis, Oregon State University, Oregon, United States of America, 1986. [Online]. Available at: https://ir.library.oregonstate.edu

[53] Standard Tables for Reference Solar Spectral Irradiances: Direct Normal and Hemispherical on 37° Tilted Surface, ASTM G173 – 03 (2020).

[54] Standard Solar Constant and Air Mass Zero Solar Spectral Irradiance Tables, ASTM E490 (2000).

[55] Photovoltaic devices - Part 3: Measurement principles for terrestrial photovoltaic (PV) solar devices with reference spectral irradiance data, IEC 60904-3:2019.

[54] Photovoltaic devices - Part 1: Measurement of photovoltaic current-voltage characteristics, IEC 60904-1:2006.

[55] Photovoltaic devices - Part 10: Methods of linearity measurement, IEC 60904-10:2007.

[56] Photovoltaic devices - Procedures for temperature and irradiance corrections to measured I-V characteristics, IEC 60891:2009.

[57] Photovoltaic devices - Part 8: Measurement of spectral response of a photovoltaic (PV) device, IEC 60904-8:1998.

[58] Photovoltaic devices - Part 2: Requirements for photovoltaic reference devices, IEC 60904-2:2015.